

Zero-frequency transport properties of one dimensional spin- $\frac{1}{2}$ systems

F. Heidrich-Meisner,^{1,*} A. Honecker,¹ D. C. Cabra,^{2,†} and W. Brenig¹

¹*Technische Universität Braunschweig, Institut für Theoretische Physik,
Mendelssohnstrasse 3, 38106 Braunschweig, Germany*

²*Ecole Normale Supérieure de Lyon, Laboratoire de Physique, Allée d'Italie, 69264 Lyon, France*
(Dated: April 25, 2003)

We report a detailed analysis of the Drude weights for both thermal and spin transport in one dimensional spin-1/2 systems by means of exact diagonalization and analytic approaches at finite temperatures. Transport properties are studied first for the integrable XXZ model and second for various nonintegrable systems such as the dimerized chain, the frustrated chain, and the spin ladder. We compare our results obtained by exact diagonalization and mean-field theory with those of the Bethe ansatz, bosonization and other numerical studies in the case of the anisotropic Heisenberg model both in the gapless and gapped regime. In particular, we find indications that the Drude weight for spin transport is finite in the thermodynamic limit for the isotropic chain. For the nonintegrable models, a finite-size analysis of the numerical data for the Drude weights is presented covering the entire parameter space of the dimerized and frustrated chain. We also discuss which conclusions can be drawn from bosonization regarding the question of whether the Drude weights are finite or not. One of our main results is that the Drude weights vanish in the thermodynamic limit for nonintegrable models.

I. INTRODUCTION

Due to their relevance for modeling the magnetic properties of several quasi-one-dimensional materials, dimerized and frustrated spin-1/2 chains and ladders are models of great and current interest. Recently, growing experimental evidence has been found that magnetic excitations can contribute significantly to the thermal conductivity of various quasi-one and quasi-two-dimensional materials^{1–11}. Stimulated by these observations, many theoretical activities have addressed the issue of heat transport in one-dimensional spin systems^{12–22}. While spin transport has been a topic of numerous theoretical investigations^{22–45}, the theory of thermal transport is less well understood.

One of the key questions is to understand under which conditions transport is ballistic, i.e., dissipationless. The criterion for this is the existence of a singularity at zero frequency in the real part of the conductivity. Therefore, one is interested in the integrated weight of this singularity - the so called Drude weight - in the thermodynamic limit. The appearance of a nonzero Drude weight is often ascribed to the influence of conservation laws on transport properties^{30,38,43,46,47}. For example, in the case of the Heisenberg chain the energy-current operator is conserved^{30,48} implying a nonzero thermal Drude weight at all temperatures. Another widely discussed and related issue is the difference between transport in integrable models compared to nonintegrable ones^{15,17,20,27,33,41,43}.

The purpose of the present paper is to provide a systematic study of both the Drude weight for spin and thermal transport at finite temperatures by means of exact diagonalization on finite systems and analytic methods. The dependence on exchange coupling anisotropy, frustration and dimerization will be clarified.

We start with an overview of the results of previous

and related works. For the anisotropic Heisenberg chain, it is possible in principle to compute thermodynamic quantities exactly with the Bethe ansatz at arbitrary temperatures. The Drude weight for thermal transport has been obtained in the antiferromagnetic regime of this model along this line^{14,49}. Numerical studies^{15,17} have provided the thermal Drude weight in the antiferromagnetic regime, in the gapped, ferromagnetic phase and for the isotropic, ferromagnetic chain. Here, we extend on such analysis by adding data for the gapless, ferromagnetic regime.

In a first numerical work devoted to the issue of thermal transport in nonintegrable models, Alvarez and Gros¹⁵ have conjectured that the Drude weight is generically finite in dimerized and frustrated spin systems although the energy-current operator is not conserved in these cases. However, we have argued in Refs. 17,21 that this conclusion cannot be sustained for gapped, frustrated chains if larger system sizes are included in the finite-size analysis. In this paper, we extend our parameter study of the thermal Drude weight to include dimerized chains and spin ladders also. The main result is that the numerical data are best interpreted in terms of a *vanishing* thermal Drude weight in nonintegrable systems.

Recently, however, the thermal Drude weight has also been computed by means of analytic approaches yielding a finite Drude weight at low temperatures^{18,20}. In Ref. 18, the spin ladder and the dimerized XY model have been studied by mapping to non-interacting models. While this is exact in the latter case, it is an approximation in the case of the spin ladder. For instance, the influence of incommensurate umklapp-scattering terms on transport properties of massive models is not yet fully understood. Bosonization was applied in Ref. 20 to the cases of the dimerized and the frustrated chain leading to the interesting result that certain umklapp-scattering

terms do not spoil the conservation of the energy current.

Spin transport in spin-1/2 models is equivalent to charge transport of (spinless) fermions and an enormous amount of work has been devoted to this field^{22–45}. The situation of spin transport in the integrable model, i.e., the Heisenberg chain, is different from the case of thermal transport since the spin-current operator is only conserved in the case of free fermions (*XY* model). Nevertheless, the Drude weight is finite in the gapless regime while numerical^{29,32} and analytical³⁶ studies have found indications that it may vanish in the gapped cases. The case of the isotropic chain is still the subject of discussion^{31,33,37,41,43,44}.

At present, no final agreement about the results from different Bethe ansatz computations^{34,37,50,51} for the Drude weight has been achieved. For example, the Bethe ansatz computations by Zotos³⁷ predict the Drude weight of the isotropic chain to be zero while Klümper and co-workers⁵⁰ have found a finite Drude weight in this case. The latter conclusion is in agreement with some numerical works - exact diagonalization^{31,33} (ED) and Quantum-Monte Carlo simulations⁴¹ (QMC) - as well as analytic approaches⁴³. Very recently, however, Long et al.⁴⁴ have developed a novel Lanczos method for finite temperatures which has been applied to spin transport in the anisotropic Heisenberg chain with up to $N = 28$ sites. They interpret their numerical results in terms of a vanishing Drude weight for the isotropic chain.

Regarding the temperature dependence of the Drude weight in the gapless regime contradicting results are reported in the literature^{37,41,43,50,51}.

As far as nonintegrable models are concerned, the effect of frustration on spin transport has been studied at zero temperature²⁶, while at finite temperatures, Ising-like interactions with distance up to 3 have been investigated with ED^{29,33} and QMC⁴¹. Fujimoto and Kawakami⁴³ have discussed transport in nonintegrable models in the low-energy limit with bosonization. They find a nonzero Drude weight provided that particle-hole symmetry is broken in agreement with Ref. 30. The physical reason is the finite overlap of the spin-current operator, which is not conserved in the presence of any umklapp scattering, to the energy-current operator.

In their work on charge transport in a one-dimensional system³⁸, Rosch and Andrei have argued that the Drude weight is zero in the presence of *dangerously irrelevant perturbations* since then all relevant conservation laws are broken. On the basis of this result, a zero Drude weight is naturally expected in all nonintegrable and gapless spin models.

It will be an additional focus of the present paper to provide a complete as possible analysis of spin transport in nonintegrable models such as the dimerized and frustrated chains as well as spin ladders. As a main result, the numerical data indicate a vanishing of the Drude weight in the thermodynamic limit consistent

with Refs. 29,38.

Although it is beyond the scope of this paper to give any conclusive explanations of recent transport experiments on low-dimensional spin materials, we will provide a list of materials for which this work could be of relevance. Whenever possible we will make connection to these experiments and discuss implications of our results for their interpretation. First, there are surprisingly large magnetic thermal conductivities observed in the compounds $(\text{Sr,La,Ca})_{14}\text{Cu}_{24}\text{O}_{41}$ ^{2–5}. Here, a strong magnetic contribution to the thermal conductivity is believed to be mediated by magnetic excitations of spin ladders. Second, similar findings have been reported for the spin chain materials SrCuO_2 , Sr_2CuO_3 ⁶ and $\text{BaCu}_2\text{Si}_2\text{O}_7$ ⁷. Third, we mention the anorganic Spin-Peierls material CuGeO_3 ¹ although the physical nature of the heat carrying excitations is still under controversial discussion^{1,52}. It has been suggested that the magnetic properties of this material can be described to some extent by a dimerized and frustrated chain. Finally, strong evidence for thermal transport mediated by magnon excitations in two-dimensional cuprate compounds has also been found^{8–11}.

The plan of the paper is the following. In Sec. II, we introduce the model which is a dimerized and frustrated Heisenberg chain including an exchange-coupling anisotropy. Next, we summarize the basic relations for the transport coefficients and, particularly, for the Drude weights as they follow from linear response theory in Sec. III. The definitions for the current operators will be given at the end of this section. Our results are presented in Secs. IV and V. First, we discuss transport properties of the anisotropic Heisenberg chain using mean-field theory and exact diagonalization. The results will be compared to Bethe ansatz computations^{14,37,49}, QMC⁴¹, and other numerical studies^{15,32,33,44} as well as analytical works^{39,43}. Second, we consider several nonintegrable models in Sec. V. Using bosonization, we argue that vanishing Drude weights are generically expected in massless³⁸ and massive nonintegrable spin models. Numerical data will be shown for both thermal and spin transport and will be related to the results of other groups^{15,18,20,43}. Finally, our main conclusions are summarized in Sec. VI.

II. MODEL

In this work we consider frustrated and dimerized spin-1/2 chains as sketched in Fig. 1. The Hamiltonian reads:

$$H = \sum_{l=1}^N h_l(\Delta, \alpha, \lambda) \quad (1)$$

$$h_l(\Delta, \alpha, \lambda) = J[\lambda_l h_{l,l+1}(\Delta) + \alpha h_{l,l+2}(\Delta)] \quad (2)$$

$$h_{l,l+i}(\Delta) = (S_l^+ S_{l+i}^- + \text{H.c.})/2 + \Delta S_l^z S_{l+i}^z. \quad (3)$$

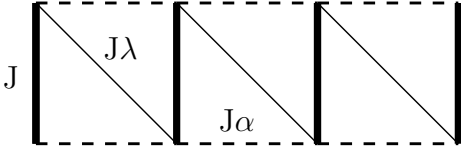


FIG. 1: Sketch of a frustrated and dimerized $S = 1/2$ chain. The limiting cases are: (i) $\alpha = 0, \lambda = 1$: the XXZ chain; (ii) $\alpha > 0, \lambda = 1$: the frustrated chain; (iii) $\alpha = 0, 0 < \lambda < 1$: the dimerized chain; (iv) $\alpha > 0, \lambda = 0$: the two-leg spin ladder.

$h_l(\Delta, \alpha, \lambda)$ from Eq. (2) is the local energy density and N the number of sites. We set $\lambda_l = 1$ if l is even and $\lambda_l = \lambda$ otherwise. In Eq. (3), $i = 1$ for nearest- and $i = 2$ for next-nearest-neighbor interactions. Throughout this work, periodic boundary conditions are used. All quantities are measured in units of the exchange coupling constant J where J is positive. Mainly, we focus on the following limiting cases of this model: (i) $\alpha = 0, \lambda = 1$, the XXZ chain; (ii) $\alpha > 0, \lambda = 1$, the frustrated chain; (iii) $\alpha = 0, 0 < \lambda < 1$, the dimerized chain; and (iv) $\alpha > 0, \lambda = 0$, the spin ladder.

We discuss various values for the anisotropy in the integrable case (i.e., $\alpha = 0, \lambda = 1$) including the XY model ($\Delta = 0$). In the case of the two-leg spin ladder ($\lambda = 0$), $\alpha = J_{\parallel}/J_{\perp}$ is equal to the ratio of the leg coupling J_{\parallel} to the rung coupling J_{\perp} .

It is instructive to write down the Hamiltonian in terms of fermionic operators. This will later be used as the starting point for the mean-field theory in Sec. IV A. By performing a Jordan-Wigner transformation (see, e.g., Ref. 53), the spin-1/2 operators $S_l^{\pm, z}$ can be mapped onto spinless fermions

$$S_l^z = c_l^\dagger c_l - \frac{1}{2}; \quad S_l^+ = e^{i\pi\Phi_l} c_l^\dagger. \quad (4)$$

$c_l^{(\dagger)}$ destroys(creates) a fermion on site l . The string operator Φ_l reads $\Phi_l = \sum_{i=1}^{l-1} c_i^\dagger c_i$. For the Hamiltonian from Eq. (1), we arrive at (see e.g., Ref. 54)

$$\begin{aligned} H = & J \sum_l \left[\frac{1}{2} \lambda_l \{ (c_l^\dagger c_{l+1} + \text{H.c.}) \right. \\ & + \Delta (c_l^\dagger c_{l+1} c_{l+1}^\dagger c_l - c_l^\dagger c_l + \frac{1}{4}) \} \\ & + \alpha \{ \frac{1}{2} (c_l^\dagger c_{l+2} + \text{H.c.}) (1 - c_{l+1}^\dagger c_{l+1}) \\ & \left. + \Delta (c_l^\dagger c_l c_{l+2}^\dagger c_{l+2} - c_l^\dagger c_l + \frac{1}{4}) \} \right]. \quad (5) \end{aligned}$$

Note the presence of correlated hopping terms, i.e., $c_l^\dagger c_{l+2} c_{l+1}^\dagger c_{l+1} + \text{H.c.}$, in Eq. (5). Such contributions are absent in the usual standard extended Hubbard models.

III. KUBO FORMULAE FOR κ AND σ

In this section we briefly review the underlying equations for the thermal and the spin conductivity and we define the energy-current operator j_{th} and the spin-current operator j_s .

A. Drude weight for heat and spin transport

The Kubo formulae for the thermal conductivity $\kappa(\omega)$ and the spin conductivity $\sigma(\omega)$ read^{53,55–57}

$$\kappa[\sigma](\omega) = \frac{[\beta]}{N} \int_0^\infty dt e^{-i(\omega+i0^+)t} \int_0^\beta d\tau \langle j_{\text{th}[s]}(-t-i\tau) j_{\text{th}[s]} \rangle. \quad (6)$$

The expressions in brackets $[\cdot]$ refer to spin transport; the index 'th' denotes thermal transport and 's' spin transport. $\beta = 1/T$ is the inverse temperature while the brackets $\langle \cdot \rangle$ denote the thermodynamic expectation value. The real part of $\kappa(\omega)$ and $\sigma(\omega)$, respectively, can be decomposed into a δ -function at $\omega = 0$ and a regular part

$$\text{Re } \kappa[\sigma](\omega) = D_{\text{th}[s]}(T) \delta(\omega) + \text{Re } \kappa[\sigma]_{\text{reg}}(\omega) \quad (7)$$

Here, we are interested in the weight $D_{\text{th}[s]}(T)$ of the δ -type singularity at $\omega = 0$. A nonzero value of $D_{\text{th}[s]}(T)$ corresponds to a divergent conductivity whereas a vanishing $D_{\text{th}[s]}(T)$ implies a normal conducting behavior if there is a contribution from the regular part of the conductivity at low frequencies or insulating behavior if $\text{Re } \kappa[\sigma]_{\text{reg}}(\omega = 0) = 0$ (see Ref. 25).

In the remainder of the paper, the dependence on system size of the Drude weight will be explicitly denoted by $D_{\text{th}[s]}(N, T)$ while $D_{\text{th}[s]}(T)$ refers to the thermodynamic limit $N \rightarrow \infty$.

A spectral representation of $\kappa[\sigma](\omega)$ in terms of eigenstates $H|n\rangle = E_n|n\rangle$ yields an expression for both Drude weights³⁰ (Z is the partition function)

$$D_{\text{th}[s]}^I(N, T) = \frac{\pi \beta^{t_{\text{th}[s]}}}{Z N} \sum_{\substack{m, n \\ E_m = E_n}} e^{-\beta E_n} |\langle m | j_{\text{th}[s]} | n \rangle|^2. \quad (8)$$

Note that the exponent $t_{\text{th}[s]}$ in the prefactor needs to be chosen according to

$$t_{\text{th}} = 2 \quad \text{or} \quad t_s = 1, \quad (9)$$

i.e., we expect $D_{\text{th}} \sim 1/T^2$ and $D_s \sim 1/T$ at high temperatures.

For spin transport, we will numerically analyze Eq. (8) and a second expression which can be derived from linear response theory^{23,27}

$$D_s^{II}(N, T) = \frac{\pi}{N} \left[\langle -\hat{T} \rangle - \frac{2}{Z} \sum_{\substack{m, n \\ E_m \neq E_n}} e^{-\beta E_n} \frac{|\langle m | j_s | n \rangle|^2}{E_n - E_m} \right]. \quad (10)$$

The operator \hat{T} is related to the kinetic energy. Note that in the derivation of Eq. (10), the f -sum rule (see Ref. 23 and references therein) is exploited. It is now instructive to make a connection to Kohn's formula for the Drude weight D_s to illustrate the relation between $D_s^I(N, T)$ and $D_s^{II}(N, T)$. As a by-product, we will obtain the appropriate definition of \hat{T} .

Equation (10) is equivalent to the generalization of Kohn's formula⁵⁸ for finite temperatures²⁷

$$D_s^{II}(T) = \frac{\pi}{ZN} \sum_n e^{-\beta E_n} \left. \frac{\partial^2 E_n(\Phi)}{\partial \Phi^2} \right|_{\Phi=0}. \quad (11)$$

To arrive at this expression, one considers finite rings of length N being pierced by the flux Φ , i.e., a static twist about the z axis. The flux-dependent Hamiltonian $H(\Phi)$ with exchange couplings $J_r \neq 0$ being nonzero for $r \leq r_0$ reads²⁶

$$H(\Phi) = \sum_{l=1}^N \sum_{r=1}^{r_0} J_r \left\{ \frac{1}{2} (e^{i(r\Phi/N)} S_l^+ S_{l+r}^- + \text{H.c.}) + \Delta S_l^z S_{l+r}^z \right\}. \quad (12)$$

Expanding $H(\Phi)$ up to second order in Φ yields^{23,26}

$$H(\Phi) = H(\Phi=0) + \frac{\Phi}{N} j_s - \frac{\Phi^2}{2N^2} \hat{T}. \quad (13)$$

The expression for the current operator j_s will be given in Sec. III B where we derive it from the equation of continuity. In terms of spin operators, \hat{T} is given by

$$\hat{T} = \sum_{l=1}^N \sum_{r=1}^{r_0} r^2 J_r (S_l^+ S_{l+r}^- + \text{H.c.}). \quad (14)$$

For the models investigated in our paper, we have $r_0 \leq 2$. In the fermionic picture (see Eq. (5)), \hat{T} is the sum of the contributions to the kinetic energy from both the nearest-neighbor and next-nearest-neighbor hopping and also the *correlated* hopping terms $c_{l+1}^\dagger c_{l+2} c_l + \text{H.c.}$. The appearance of the extra factor of 4 in front of the term proportional to $J_2 = \alpha J$, which arises from the factor r^2 in Eq. (14), can be understood by considering the limit of two decoupled chains ($J\alpha = \text{const}; J \rightarrow 0$) of length $N/2$. Rescaling the size-dependent prefactors in Eq. (13) on $N/2$ cancels the factor of 4 and results in twice the Hamiltonian of a single chain with $N/2$ sites. By applying second-order perturbation theory to $H(\Phi)$ it is straightforward to arrive at Eq. (10) (see, e.g., Ref. 23).

The relation between $D_s^I(N, T)$ and $D_s^{II}(N, T)$ has been pointed out in Refs. 25,30,33,35. While

$$D_s(T) = \lim_{N \rightarrow \infty} D_s^I(N, T) = \lim_{N \rightarrow \infty} D_s^{II}(N, T)$$

holds for all temperatures $T > 0$ in the thermodynamic limit, the two expressions are not equivalent on *finite* systems. For instance, Eq. (10) may result in negative

values on finite systems at $T = 0$ (see Refs. 24,35 for examples) whereas $D_s^I(N, T) \geq 0$ is strictly fulfilled by evaluation of Eq. (8) (see, e.g., Ref. 30 for details). Note in this context that the difference $D_s^{II}(N, T) - D_s^I(N, T)$ is proportional to the second derivative of the free energy with respect to the flux Φ in the limit of vanishing momentum. In general, this quantity measures the superfluid density^{25,30,35} in more than one spatial dimension. However, for a one-dimensional model, it vanishes in the thermodynamic limit^{30,35}.

Eq. (8) can also be related to Kohn's formula. While the latter one is the sum of the curvature of energy levels, $D_s^I(N, T)$ equals the sum of squares of first derivatives of the energy levels with respect to the flux Φ ³³

$$D_s^I(N, T) = \frac{\pi}{ZN} \sum_n e^{-\beta E_n} \left(\left. \frac{\partial E_n(\Phi)}{\partial \Phi} \right|_{\Phi=0} \right)^2. \quad (15)$$

In this paper, Eqs. (8) and (10) will be used to compute the Drude weights while Eqs. (11) and (15) have been given for completeness. We will show in Sec. IV B 3 that the difference between $D_s^I(N, T)$ and $D_s^{II}(N, T)$ is negligibly small at sufficiently high temperatures already on finite systems. At low temperatures, only $D_s^{II}(N, T)$ yields a good description of the temperature dependence.

If the current operator $j_{\text{th}[s]}$ is a conserved quantity, Eq. (8) can be rewritten as

$$D_{\text{th}[s]}^I(N, T) = \frac{\pi \beta^{t_{\text{th}[s]}}}{ZN} \sum_n e^{-\beta E_n} \langle n | j_{\text{th}[s]}^2 | n \rangle \quad (16)$$

$$= \frac{\pi \beta^{t_{\text{th}[s]}}}{N} \langle j_{\text{th}[s]}^2 \rangle, \quad (17)$$

implying that a *static* expectation value has to be computed which is a considerable simplification. Analogously, we obtain

$$D_s^{II}(N, T) = \frac{\pi}{N} \langle -\hat{T} \rangle. \quad (18)$$

from Eq. (10) under the condition $[H, j_s] = 0$. The main goal of this work is to investigate whether $D_{\text{th}[s]}$ has a finite value in the thermodynamic limit ($N \rightarrow \infty$). Typically, the finite-size dependence is well controlled at high temperatures $T \gg J$ where all states $|n\rangle$ are occupied with equal probability $e^{-\beta E_n} \rightarrow 1$. In this case, we see from Eq. (8) that

$$\lim_{T \rightarrow \infty} [T^{t_{\text{th}[s]}} D_{\text{th}[s]}^I(N, T)] = C_{\text{th}[s]}(N) \quad (19)$$

with a prefactor $C_{\text{th}[s]}$

$$C_{\text{th}[s]}(N) = \frac{\pi}{Z_\infty N} \sum_{\substack{m,n \\ E_m = E_n}} |\langle m | j_{\text{th}[s]} | n \rangle|^2. \quad (20)$$

In the limit $T \rightarrow \infty$, the partition function $Z_\infty = 2^N$ is equal to the dimension of the Hilbert space.

B. The current operators

The current operators obey the following equations of continuity

$$\partial_t h_l = i[H, h_l] = -(j_{\text{th},l+1} - j_{\text{th},l}) \quad (21)$$

$$\partial_t S_l^z = i[H, S_l^z] = -(j_{s,l+1} - j_{s,l}) \quad (22)$$

where h_l is the local energy density, S_l^z the local magnetization density and $j_{\text{th}[s],l}$ are the local current operators. From Eqs. (21) and (22), we obtain solutions for the current operators for arbitrarily long-ranged interactions. If $[h_{l\pm r}, h_l] \neq 0$ holds only for $r \leq r_0$, the energy-current operator reads^{17,48,59}

$$j_{\text{th}} = \sum_{l=1}^N j_{\text{th},l} = i \sum_{l=1}^N \sum_{n,r=0}^{r_0-1} [h_{l-r-1}, h_{l+n}]. \quad (23)$$

The spin current is given by^{23,26}

$$j_s = \sum_{l=1}^N j_{s,l} = i \sum_{l=1}^N \sum_{n,r=0}^{r_0-1} [h_{l-r-1}, S_{l+n}^z]. \quad (24)$$

with $[h_{l-r}, S_l^z] \neq 0$ for $r \leq r_0$. In this paper, we restrict ourselves to $r_0 \leq 2$. The same result can be obtained from Eq. (13). Independent of the model, the local magnetization density is given by S_l^z whereas we use Eqs. (2) and (3) as a definition for the local energy density. For the XY model, both quantities j_{th} and j_s commute with the Hamiltonian, i.e., $[H^{XY}, j_{\text{th}[s]}] = 0$. While $[H^{XXZ}, j_{\text{th}}] = 0$ remains valid for arbitrary Δ and $\alpha = 0$; $\lambda = 1$ ^{30,48}, the conservation of j_s is immediately broken once the anisotropy Δ has a nonzero value. Dimerization and frustration which spoil the integrability of the XXZ model also lead to $[H, j_{\text{th}[s]}] \neq 0$ (except for $\Delta = \alpha = 0$).

IV. XXZ MODEL

In this section we discuss transport properties of the XXZ model. Since this model is solvable via the Bethe ansatz, certain thermodynamic quantities like susceptibility^{60,61} or specific heat^{14,61} are accessible with this technique. The thermal Drude weight D_{th} has recently been computed along this line by Klümper and Sakai^{14,49} for arbitrary $\Delta \geq 0$. For spin transport, finite-temperature Bethe ansatz computations have been performed by both Zotos³⁷ and Klümper and coworkers⁵⁰. However, these two groups find different results for the temperature dependence which is ascribed to conceptual problems of computing the Drude weight from a single microstate at a given temperature^{51,62}.

First, we apply mean-field theory based on the Jordan-Wigner transformation and compute the Drude weights in the gapless, antiferromagnetic regime $0 \leq \Delta \leq 1$. This approach yields a good approximation to the exact results from the Bethe ansatz (compare Ref. 17) for the

thermal conductivity whereas for spin transport, it fails to describe the Δ -dependence of the Drude weight D_s . Second, we present our results from exact diagonalization focusing mainly on spin transport.

A. Mean-field theory

In this section, we consider an approximate treatment of the Hamiltonian of the anisotropic chain within mean-field theory. First, this approach will provide exact expressions for the Drude weights in the case of free fermions ($\Delta = 0$) which is useful for a check of the numerical implementation. Second, we will see that the thermal Drude weight of the XXZ chain can be well described by this approximation for $|\Delta| \leq 1$ ¹⁷ which is, however, not the case for spin-transport.

Within mean-field theory, the interaction terms in the fermionized Hamiltonian from Eq. (5) are simplified by means of a Hartree-Fock decomposition. Since details of the procedure can be found in the literature (see, e.g., Ref. 54), we prefer to quote directly the result for the mean-field Hamiltonian (k labels the momentum)

$$H_{\text{MF}} = \sum_k \epsilon_k c_k^\dagger c_k. \quad (25)$$

H_{MF} is diagonal in momentum space with the tight-binding dispersion

$$\epsilon_k = -t(\Delta, T) \cos(k). \quad (26)$$

The hopping amplitude $t(\Delta, T) := -(1 + 2A(T)\Delta)$ is modified via the one-particle expectation value

$$A(T) = \langle c_l^\dagger c_{l+1} \rangle = \frac{1}{\pi} \int_0^\pi dk \cos(k) f(\epsilon_k), \quad (27)$$

which needs to be determined self-consistently. Note that $f(\epsilon) = 1/(\exp(\beta\epsilon) + 1)$ is the Fermi function.

In the mean-field description, the current operators are simply given by

$$j_{\text{th}}^{\text{MF}} = \sum_k \epsilon_k v_k n_k; \quad j_s^{\text{MF}} = \sum_k v_k n_k, \quad (28)$$

with velocity $v_k = \partial \epsilon_k / \partial k$ and $n_k = c_k^\dagger c_k$. The spinon velocity, i.e., $v_0^{\text{MF}} = v_k(T = 0)$, follows from Eq. (26) $v_0^{\text{MF}} = 1 + 2A(T = 0) \cdot \Delta$ with $A(T = 0) = 1/\pi$. From Eq. (17), we obtain the Drude weights

$$D_{\text{th}}^{\text{MF}}(T) = \frac{\pi}{NT^2} \sum_k (\epsilon_k v_k)^2 f^2(\epsilon_k) e^{\epsilon_k/T}, \quad (29)$$

$$D_s^{\text{MF}}(T) = \frac{\pi}{NT} \sum_k v_k^2 f^2(\epsilon_k) e^{\epsilon_k/T}. \quad (30)$$

In the case of free fermions, i.e., $\Delta = 0$, Eqs. (29) and (30) are exact and can be evaluated both on finite systems and in the thermodynamic limit. This provides a

useful check for the numerical implementation; in particular since the spin-current operator j_s is independent of Δ (see Eq. (24)).

For thermal transport, the mean-field approach provides a good approximation to $D_{\text{th}}(T)$ for $|\Delta| \leq 1$ as we have shown in Ref. 17 and as can be seen in the inset of Fig. 2 (a) where we compare $D_{\text{th}}(T)$ from the mean-field approach (dotted line) with the Bethe ansatz results from Ref. 14 (solid line) for $\Delta = 0.5$.

Regarding the spin transport, we note that the mean-field theory does not give a qualitatively correct description of $D_s(\Delta)$. Equation (30) results in $D_s^{\text{MF}}(T=0) = v_0^{\text{MF}}(\Delta)$. Basically, the Drude weight increases with Δ here because $D_s^{\text{MF}} \sim \langle -\hat{T} \rangle$ essentially measures the increase of the bandwidth with Δ . This is in contrast to the exact expression for $D_s(T=0)$ ²³

$$D_s(T=0) = \frac{\pi^2}{4} \frac{\sin(\gamma)}{\gamma(\pi - \gamma)}; \quad \Delta = \cos(\gamma) \quad (31)$$

where D_s decreases with Δ due to the presence of the interaction terms in Eq. (5). The reason for the failure of the mean-field theory is that the current operator j_s^{MF} is conserved for $0 \leq \Delta \leq 1$ which is not true for the full Hamiltonian (1) and the respective current operator (24). Note that the exact Drude weight takes the form $D_s(T=0) \sim K v_0$ where K is the Luttinger parameter and v_0 the velocity at $T=0$ (see, e.g., Ref. 39). It is precisely the factor of K that is missing in the mean-field result.

B. Numerical results for the XXZ model

Now we turn to the discussion of the results from exact diagonalization for (i) the thermal Drude weight D_{th} and (ii) the Drude weight D_s for spin transport of the anisotropic chain. Before going into details, let us outline the structure of this section and point out the main results:

First, we discuss technical aspects of the numerical procedure which will also be of relevance for the nonintegrable models in Sec. V. In particular, the importance of degenerate states and their numerical identification will be emphasized.

Second, the numerical results for the thermal Drude weight $D_{\text{th}}(N, T)$ for $\Delta = \pm 0.5, 2$ will be presented and compared to the Bethe ansatz^{14,49}. In addition, the high-temperature prefactor C_{th} is computed and discussed as a function of Δ .

Third, a detailed parameter study of the Drude weight D_s is performed. Results for $D_s^{I,II}(N, T)$ are shown for $\Delta = 0.5, \pm 1, -2$ as well as for $\Delta > 1$. We discuss the temperature dependence of both $D_s^I(N, T)$ and $D_s^{II}(N, T)$ and point out that they are indistinguishable at high temperatures, but exhibit a completely different finite-size scaling³³ at low T . This result, i.e., $D_s^I(N, T) = D_s^{II}(N, T)$ for T large enough, is of importance since the Drude weight could in principle also be

obtained analytically from Eq. (8) or (15), respectively, which has to our knowledge not been attempted so far. Further, the influence of logarithmic finite-size corrections at $T=0$ for the isotropic chain is mentioned³⁹. Finally, and most important, we analyze the finite-size scaling of the high-temperature prefactor C_s and its dependence on Δ . While we can unambiguously confirm that $\lim_{N \rightarrow \infty} C_s(N) > 0$ for $|\Delta| < 1$ in agreement with the results of other groups^{29,32,33,37,41,43,44}, the data for $\Delta = 1$ clearly indicate a *finite* Drude weight $D_s(T > 0)$ as well. The latter observation is in agreement with Refs.^{31,33,41,43,50} but contradicts the conclusions of Refs.^{37,44}.

1. Technical remarks on the numerical procedure

We start with several technical remarks on the numerical procedure which are relevant for both integrable and nonintegrable models. We have performed complete diagonalization for chains with $N \leq 18$ sites exploiting conservation of the z -component $S_{\text{tot}}^z = \sum_l S_l^z$ of the total spin, translational invariance, and spin-inversion symmetry in the $S^z = 0$ subspaces of systems with even N . The latter symmetry is respected by the energy-current operator j_{th} but not by the spin-current operator j_s . The dimensions of the largest subspaces for a given momentum k are ≈ 2400 for $S_{\text{tot}}^z = 1$ and ≈ 2700 for $S_{\text{tot}}^z = 0$ at $N = 18$. In the latter case, the dimension is almost reduced by a factor of 2 by spin-inversion symmetry for the subspaces with odd and even sign under this symmetry.

Another important aspect is the identification of degenerate states (i.e., $E_n = E_m$) in subspaces labeled by S_{tot}^z and momentum k . This is necessary both in the evaluation of Eqs. (8) and (10) but becomes irrelevant if the respective current operator is conserved, leading to the simpler expression, Eq. (16). The latter is possible for thermal transport in the XXZ model.

For spin transport, however, we have $[H, j_s] \neq 0$ for $\Delta \neq 0$. The (integrated) distribution of level spacings ΔE_n is shown in Fig. 3. There, the number $I(\epsilon)$ of level spacings $\Delta E_n = E_{n+1} - E_n$, $E_n < E_{n+1}$ of adjacent energy levels being smaller than a given value of ϵ is plotted versus ϵ for $\Delta = 0.5$

$$I(\epsilon) = \sum_{(S_{\text{tot}}^z, k)} \sum_{\Delta E_n < \epsilon} 1. \quad (32)$$

It is sufficient to analyze all subspaces with given S_{tot}^z and momentum k separately and sum over all subspaces thereafter (indicated by the first sum in Eq. (32)).

The spectrum displays some characteristic features: first, the value of $I(\epsilon)$ for $\epsilon \rightarrow \infty$ equals the dimension of the Hilbert space 2^N minus the number of subspaces (S_{tot}^z, k) . Second, a large fraction of degenerate states is present and third, the integrated distribution of level spacings is constant for $10^{-9}J \lesssim \epsilon \lesssim 10^{-6}J$ for the system sizes investigated here. This suggests that adjacent energy levels

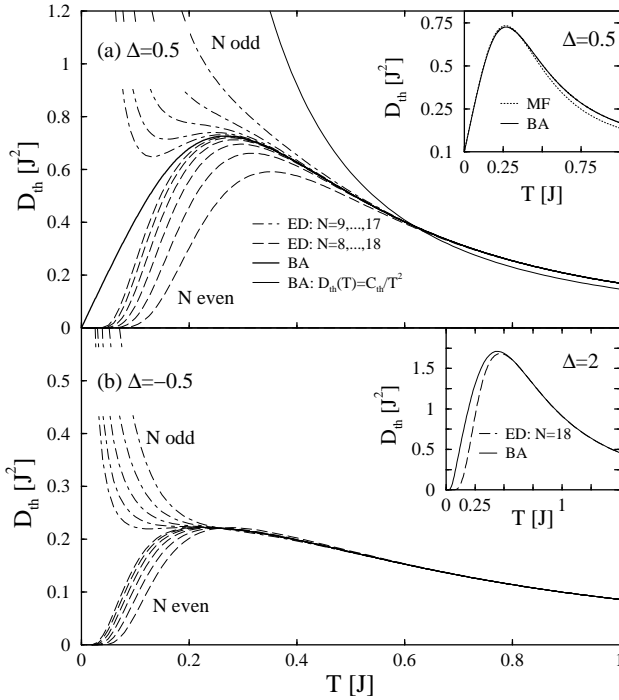


FIG. 2: Thermal Drude weight of the XXZ chain for: $\Delta = 0.5$ (panel (a)), $\Delta = -0.5$ (panel (b)) and $\Delta = 2$ (inset in panel (b)). Dashed(dot-dashed) lines: ED data for even(odd) N . Solid lines: Bethe ansatz (BA) results from Refs. 14, 49. Thin, solid line in (a): high-temperature limit $D_{\text{th}}(T) \simeq C_{\text{th}}/T^2$ from Ref. 14. Dotted line in the inset of (a): mean-field (MF) approximation.

are typically separated by $\Delta E_n \lesssim 10^{-9}J$ if they are degenerate.

This separation allows for an identification of degenerate states by imposing the following criterion in the numerical analysis: energy levels with $|E_{n+1} - E_n| < \epsilon_{\text{cut}} = 10^{-8}J$ are degenerate. By evaluation of Eq. (8) for the thermal Drude weight we find agreement with Eq. (16) and the Bethe ansatz¹⁴ for this choice of ϵ_{cut} but significant deviations at temperatures $T \sim J$ if larger or lower values for the cutoff energy are used.

2. Thermal transport in the XXZ model

Numerical results for the thermal Drude weight $D_{\text{th}}(N, T)$ have previously been presented for $\Delta = 1$ in Refs. 15, 17 and for $\Delta = -1, -2, 10$ in Ref. 17. We enhance on the latter study by adding numerical data for the gapless antiferromagnetic and the ferromagnetic regime which is shown in Fig. 2 (panel (a): $\Delta = 0.5$, (b) $\Delta = -0.5$). Dashed(dot-dashed) lines display ED-data for N even(odd). Since we are using periodic boundary conditions, the twofold degeneracy of the ground state for chains with an odd number of sites leads to a divergence of $D_{\text{th}}(N, T)$ for $T \rightarrow 0$. The Drude weight of systems with an even number of sites is characterized by an exponential suppression $D_{\text{th}}(N, T) \sim e^{-\Delta_{\text{FS}}/T}$ at low

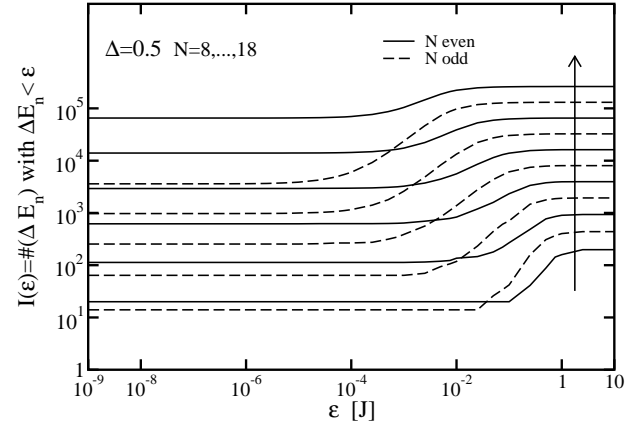


FIG. 3: Distribution of level spacings in the spectrum of finite chains with $8 \leq N \leq 18$ (bottom to top as indicated by the arrow) for $\Delta = 0.5$ (solid lines: N even, dashed lines: N odd). ΔE_n is the difference of adjacent energy levels in subspaces classified by total S_{tot}^z and momentum k . The number $I(\epsilon)$ of ΔE_n with $\Delta E_n < \epsilon$ summed over all subspaces is plotted versus ϵ (see Eq. (32)).

temperatures where Δ_{FS} is the finite-size gap of the system.

A striking feature of $D_{\text{th}}(N, T)$ of the XXZ model is the rapid convergence with N at high temperatures. The difference between the numerical data for the largest system investigated for $\Delta = 0.5$ (i.e., $N = 18$) and the Bethe ansatz curve¹⁴ (solid line in Fig. 2 (a)) is smaller than $10^{-2}J^2$ for temperatures $T \gtrsim 0.23J$. Basically, the convergence of the numerical data is as good as in the case of other thermodynamic quantities such as specific heat C_V and susceptibility χ . We stress that the relation $D_{\text{th}}(T) \sim C_V(T)$ only holds at high and low temperatures (see Ref. 14).

The antiferromagnetic, gapped regime has been discussed in Ref. 17. We mention that in the meantime Bethe ansatz computations⁴⁹ have been extended to $\Delta > 1$. The numerical data are in agreement with these results (see inset of Fig. 2 (b): solid line, BA; dashed line, ED for $N = 18$ at $\Delta = 2$).

We continue by a discussion of the high-temperature prefactor C_{th} defined in Eq. (19). As is evident from Fig. 2 (a) and (b), the value of $C_{\text{th}} := \lim_{N \rightarrow \infty} C_{\text{th}}(N)$ can be numerically determined already from systems with a comparably small number of sites (e.g., $N = 12$) with very good accuracy. Here we are interested in the Δ -dependence of C_{th} as shown in Fig. 4 (squares: ED). Note the excellent agreement with the analytic expression from the Bethe ansatz¹⁴ (solid line in Fig. 4)

$$C_{\text{th}}(\Delta) = \frac{\pi J^4}{64} \left(3 + \frac{\sin(3 \arccos(\Delta))}{\sin(\arccos(\Delta))} \right). \quad (33)$$

For $\Delta = 0$ (i.e., free fermions), we get $C_{\text{th}}(\Delta = 0) = \pi J^4/32$ which can also be obtained from Eq. (29).

There are two main features of $C_{\text{th}}(\Delta)$: (i) $C_{\text{th}}(\Delta) = C_{\text{th}}(-\Delta)$ (see Fig. 4 (a)) and (ii) $\lim_{\Delta \rightarrow \infty} [C_{\text{th}}(\Delta)/\Delta^4] =$

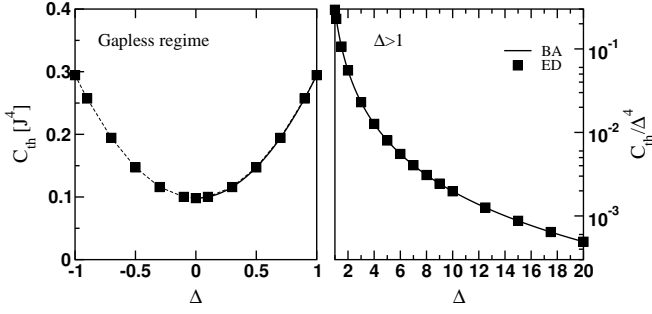


FIG. 4: High-temperature prefactor C_{th} for the XXZ model in the gapless (left panel) ($|\Delta| \leq 1$) and gapped, antiferromagnetic regime (right panel) ($\Delta > 1$). The numerical data (ED) are in perfect agreement with the exact expression for C_{th} from the Bethe ansatz¹⁴ (BA).

0 (see Fig. 4 (b)). In Fig. 4 (b), C_{th} is measured in units of Δ .

The first property can be seen from the following observations: changing the sign of Δ is an antiunitary transformation and essentially turns $H(-\Delta) = -H(\Delta)$ and $E_n(-\Delta) = -E_n(\Delta)$ while the eigenvectors remain unchanged (this follows from an additional rotation by π about the z axis on all sites with even site index). This transformation leaves the energy-current operator unchanged, i.e., $j_{th}(-\Delta) = j_{th}(\Delta)$. From Eq. (20), we can then conclude $C_{th}(\Delta) = C_{th}(-\Delta)$.

For $J/\Delta \rightarrow 0$, the Ising limit $H = \sum_l S_l^z S_{l+1}^z$ is approached where the only possible excitations are local spin flips. Here, no current can flow and, consistent with this notion, $[h_l, h_{l+1}] = 0$ leading to $j_{th} \equiv 0$ (see Eq. (23)) and $D_{th} \equiv 0$ for $J/\Delta = 0$.

3. Spin transport in the XXZ model

In the following, a survey of the results for D_s for arbitrary values of the anisotropy will be given. First, the gapless, antiferromagnetic regime ($0 < \Delta \leq 1$; Fig. 5) will be discussed with a particular focus on the isotropic chain ($\Delta = 1$). Second, we comment on the finite-size data for D_s for the gapped, antiferromagnetic case ($\Delta > 1$; Fig. 6 (a), (b)), and third, results for the ferromagnetic regime will be shown ($\Delta < 0$; Fig. 6 (c), (d)). Finally, the dependence of the high-temperature prefactor C_s on both anisotropy and system size is analyzed (Fig. 7).

Numerical results for $D_s^{I,II}(N, T)$ in the gapless, antiferromagnetic regime are shown in Fig. 5 for $\Delta = 0.5$ (panel (a)) and $\Delta = 1$ (panel (b)). Note that our results for $D_s^I(N, T)$ agree with the data for $\Delta = 0.4$ (not shown in the figures) and $N \leq 14$ published in Ref. 33 by Narozhny et al.

First, we concentrate on the case of $\Delta = 0.5$. In panel (a), we compare data from Eqs. (8) ($D_s^I(N, T)$, dashed lines) and (10) ($D_s^{II}(N, T)$, solid lines) confirming that these two expressions are equivalent at high temperatures

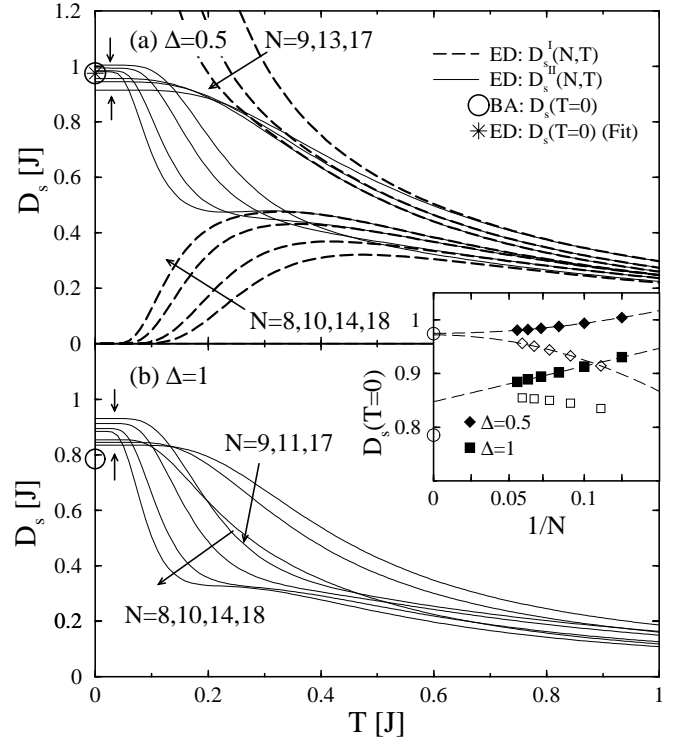


FIG. 5: Spin transport: Drude weight for $\Delta = 0.5$ (panel (a)) and $\Delta = 1$ (panel (b)). Dashed lines are numerical data obtained for $D_s^I(N, T)$ from Eq. (8); solid lines denote $D_s^{II}(N, T)$ from Eq. (10). Arrows indicate increasing system size. Note that $D_s^{II}(N, T)$ shows a better convergence with N at low temperatures compared to $D_s^I(N, T)$. The inset shows the Drude weight at $T = 0$ for $\Delta = 0.5$ (diamonds) and $\Delta = 1$ (squares) as a function of the inverse system size. The dashed lines are fits applied to the subsets with even (solid symbols) and odd (open symbols) N . Open circles at $T = 0$ denote the exact values for $D_s(T = 0)$ ²³.

($T \gtrsim 0.5J$, depending on system size).

At low temperatures, $D_s^I(N, T)$ shows much slower convergence with N and essential features of the temperature dependence are only present in the data for $D_s^{II}(N, T)$ which are the finite value at $T = 0$ and the vanishing slope of $D_s^{II}(N, T)$ for $T \rightarrow 0$. The latter observation (i.e., $dD_s^{II}(N, T)/dT = 0$ at $T = 0$) is consistent with the Bethe ansatz by Klümper and co-workers^{50,51}. In general, the functional form of $D_s(T)$ at low T for $|\Delta| < 1$ is

$$D_s(T) = D_s(T = 0) - \text{const} \cdot T^\alpha \quad (34)$$

where the exponent α depends on the anisotropy. In Ref. 37, the expression $\alpha = \frac{2}{\nu-1}$ was derived (The integer ν parameterizes the anisotropy via $\Delta = \cos(\pi/\nu)$). Taking this result, Eq. (34) would imply $D_s(T) = D_s(T = 0) - \text{const} \cdot T$ for $\Delta = 0.5$ which is obviously not consistent with our numerical data. For $|\Delta| < 1$ and low T , the temperature dependence seems to be described by the expressions derived by Fujimoto and Kawakami⁴³

which are compatible with QMC⁴¹ and the ED presented here.

We have also determined $D_s^{II}(N, T = 0)$ numerically by evaluating Eq. (10) in the subspace containing the ground state (see inset of Fig. 5). Using Eq. (11), one could go to larger systems than $N = 18$ since only the curvature of the ground state is needed. However, the main topic of this work is the Drude weight at finite temperatures while the finite-size corrections for the $T = 0$ Drude weight have been computed in Ref. 39.

Data for $D_s^{II}(N, T = 0)$ are plotted versus $1/N$ in the inset of Fig. 5 for $\Delta = 0.5$ (diamonds) and $\Delta = 1$ (squares). The data from finite systems with an even number of sites form a monotonically decreasing sequence with N at $T = 0$ and small temperatures (see Fig. 5 (a), $T \lesssim 0.2J$) while the data for odd N are a monotonically increasing sequence. Thus, the results for $D_s^{II}(N, T)$ and even N provide an upper bound and those from systems with odd N a lower bound for $D_s(T)$ at low temperatures. From Ref. 39, the leading finite-size corrections at $T = 0$ are available

$$D_s^{II}(N, T = 0) = D_s(T = 0) + \frac{B}{N^\mu} + \dots \quad (35)$$

with $\mu = 2$ for $\Delta \lesssim 0.5$. Performing fits according to Eq. (35) at $T = 0$ separately for even(odd) N results in $D_s(T = 0) = 0.9747(0.9717)J$ for $\Delta = 0.5$ which is in very good agreement with the exact result²³ $D_s(T = 0) = 0.97428J$.

At the isotropic point, i.e., $\Delta = 1$, the curves display similar features as for $\Delta = 0.5$: (i) a vanishing slope for $T \rightarrow 0$, (ii) a monotonic decrease at high temperatures, and (iii) $D_s^{II}(2N, T) < D_s^{II}(2N - 2, T)$ ($D_s^{II}(2N + 1, T) > D_s^{II}(2N - 1, T)$) at low temperatures $T \lesssim 0.1J$.

However, the finite-size data at the isotropic point and $T = 0$ seem to follow $D_s^{II}(N, T = 0) = A + B/N$ in contrast to the case of $\Delta = 0.5$ as can be seen in the inset of Fig. 5 (b). For A , we find $A \approx 0.847J$ which compares well with numerical results obtained by the Lanczos method reported in Ref. 26. Admittedly, a good approximation to the exact value of $D_s(T = 0)$ at $\Delta = 1$ for $N \rightarrow \infty$ cannot be obtained from the numerical data since the system sizes are far too small (see Fig. 5 (b)). In fact, from the work of Laflorencie et al.³⁹ it is known that the relevant and leading finite-size correction at $T = 0$ and $\Delta = 1$ is a logarithmic term. This is because umklapp scattering is a marginally irrelevant perturbation in this case. Similar to the susceptibility $\chi(T)$ ^{39,60}, $D_s(T)$ is expected to show a sharp drop for $T \rightarrow 0$ accompanied with a diverging slope at $T = 0$ ⁵⁰ in the thermodynamic limit.

At sufficient large temperatures, we believe that the numerical data for $\Delta = 1$ presented in Fig. 5 (b) give the correct picture of the temperature dependence of the Drude weight. However, Fujimoto and Kawakami⁴³ have recently obtained an analytic expression for $D_s(T)$ in the low-energy limit with conformal field theory which

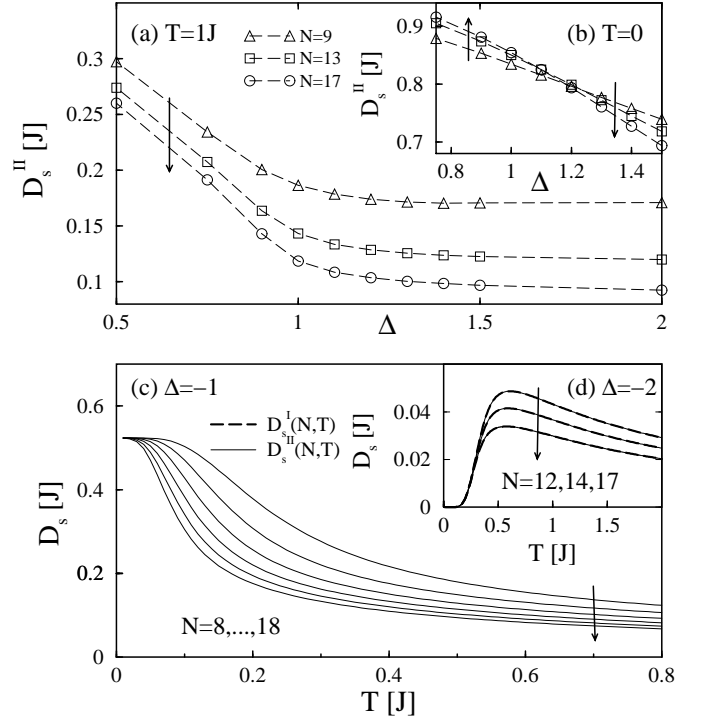


FIG. 6: Spin transport. Panels (a) and (b): Drude weight $D_s^{II}(N, T)$ as a function of Δ . ($N = 9, 13, 17$; in (a): $T = 1J$; (b): $T = 0$). Panel (c): Drude weight $D_s^{II}(N, T)$ for $\Delta = -1$ and $8 \leq N \leq 18$ (N even, top to bottom). Panel (d): Drude weight for $\Delta = -2$ and $N = 12, 14, 17$ (top to bottom; dashed lines: $D_s^I(N, T)$ Eq. (8), solid lines: $D_s^{II}(N, T)$ Eq. (10)). Arrows indicate increasing system size.

is compatible with our numerical data for $|\Delta| < 1$ but not for $\Delta = 1$. Here, Fujimoto and Kawakami find $D_s(T) < D_s(T = 0)$ while the data shown in Fig. 5 (b) seemingly support the opposite relation. Despite this discrepancy, our results do nevertheless support the notion of a *finite* $D_s(T > 0)$ at $\Delta = 1$. This is substantiated by the analysis of the high-temperature prefactor $C_s(N)$ (see Eq. (20)) as we will discuss in detail below.

For larger Δ (i.e., $\Delta > 1$), the monotonic increase of $D_s^{II}(N, T)$ at low temperatures for odd N changes to a monotonic decrease. This is illustrated in Fig. 6 (b) where $D_s^{II}(N, T = 0)$ is plotted versus Δ for $N = 9, 13, 17$ (compare Refs. 39,63). The cross-over in the monotony occurs at $\Delta \approx 1.2$, i.e., in the gapped regime. Since $D_s^{II}(N, T) \approx \text{const}$ for small T , the behavior at $T = 0$ is characteristic for the low-temperature regime. At larger temperatures, $D_s^{II}(N, T)$ is a monotonically decreasing function for both even and odd N (see panel (a) of Fig. 6 for odd N and $T = 1J$).

Regarding the ferromagnetic regime (i.e., $\Delta < 0$), we concentrate on $\Delta = -1$ and $\Delta = -2$. The results for $\Delta = -1$ plotted in Fig. 6 (c) indicate $D_s^{II}(N, T) \approx \text{const}$ at low T with $D_s(T = 0) \approx 0.523(5)J$. However, since the low-energy spectrum for $\Delta = -1$ is of comparable complexity as for $\Delta = 1$, one may expect nontrivial finite-

size corrections which could lead to a different temperature dependence at low T . If the latter is true, then the system sizes are too small to draw conclusions about the behavior of $D_s^{II}(N, T)$ at very low T .

The Drude weight in the gapped, ferromagnetic regime is expected to show a behavior analogous to that of $\Delta > 1$. For instance, $D_s^{II}(N, T)$ is monotonically decreasing with N at all temperatures irrespective of odd-even effects. Interestingly, $D_s^I(N, T)$ and $D_s^{II}(N, T)$ turn out to be indistinguishable for $\Delta < -1$ and N large enough which is illustrated in Fig. 6 (d). This plot shows $D_s^{I,II}(N, T)$ for $N = 12, 14, 17$ at $\Delta = -2$ where dashed lines denote $D_s^I(N, T)$ from Eq. (8) and solid lines stem from Eq. (10) ($D_s^{II}(N, T)$).

To conclude this section, we discuss the high-temperature prefactor C_s both as a function of anisotropy and system size. In Fig. 7 (a), $C_s(N)$ is shown versus $1/N$ for $\Delta = 0, 0.5, 0.6, 1, 1.5$. Results for the case of free fermions ($\Delta = 0$) have been deduced from Eq. (30) on finite systems in the fermionic picture. To fix the absolute values we note that $C_s = \pi/8$ in our notation for the free-fermion case $\Delta = 0$.

As is evident from Fig. 7 (a), $C_s(N)$ roughly follows

$$C_s(N) = a + \frac{b}{N} + \dots \quad (36)$$

The same finite-size extrapolation has been used for $D_s^I(N, T) \cdot T$ in Ref. 33 for even-numbered systems and $N \leq 14$ at $T = 50J$. However, by comparing the direct computation of $C_s(N)$ from Eq. (20) with fitting

$$D_s^{I,II}(N, T) = \frac{C_s(N)}{T} + \frac{C_1(N)}{T^2} + \dots \quad (37)$$

to $D_s^{I,II}(N, T)$, we find that, often, more than one term in Eq. (37) needs to be taken into account to recover the result for $C_s(N)$ from Eq. (20). Consequently, it is preferable to compute $C_s(N)$ directly from Eq. (20). The data can be well extrapolated according to Eq. (36) for $\Delta = 0.5$ and $\Delta \geq 1$. A subtlety arises from the strong differences between even and odd-numbered systems for intermediate values of Δ such as $\Delta = 0.6$ (see Fig. 7 (a)). In these cases (i.e., $\Delta = 0.2, 0.4, 0.6, 0.8, 0.9$) we have separately performed fits to the subsets with even and odd N . C_s is then estimated by averaging the results from the fits. The large error bars for $\Delta = 0.2, 0.4, 0.6, 0.8, 0.9$ are due to these large differences in the extrapolated values of subsets with even and odd N .

Following this procedure, we obtain $C_s = (0.15 \pm 0.03)J^2$ for $\Delta = 0.6$ while the extrapolation of the even-numbered systems yields $C_s = (0.123 \pm 0.001)J^2$. The latter value compares well to the data published in Ref. 33 ($C_s = (0.119 \pm 0.004)J^2$). The strong finite-size effects between even and odd numbered systems, however, indicate that additional finite-size corrections apart from a simple $1/N$ -term must become relevant for larger N if the sequences of even and odd N converge to the same value in the thermodynamic limit. A difference in the extrapolated value for large N of these two subsets does

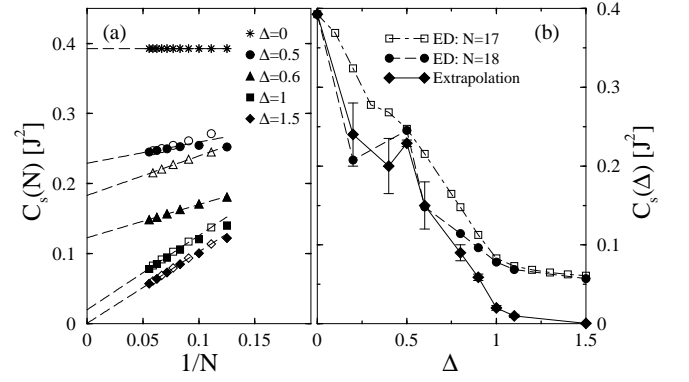


FIG. 7: Spin transport. Panel (a): high-temperature prefactor $C_s(N)$ versus $1/N$ for $\Delta = 0, 0.5, 0.6, 1, 1.5$ (solid(open) symbols: even(odd) N). The dashed lines are fits according to Eq. (36) (see text for details). Panel (b): extrapolated high-temperature weight $C_s(\Delta)$ as a function of the anisotropy Δ (diamonds) and the data for $N = 17, 18$ (squares, circles). The lines are guides to the eyes.

not seem to be plausible.

Note that it has been suggested in Refs. 32,44 to partly include spectral weight from low frequencies of $\text{Re} \sigma(\omega)$ to obtain C_s for all those Δ which cannot be written as $\Delta = \cos(\pi/\nu)$, ν integer. However, within such a procedure, a criterion is necessary to decide up to which frequency one should integrate $\text{Re} \sigma(\omega)$ and it goes obviously beyond the usual definition of the Drude weight via Kohn's formula (11). In this paper, we prefer to confine our analysis to Eq. (10), or (11) respectively.

At the isotropic point $\Delta = 1$, we have fitted the numerical data for $C_s(N)$ using Eq. (36) while varying the range of data points ($N_{\min} \leq N \leq N_{\max}$). Stable fit results are obtained for $11 \leq N \leq N_{\max}$ with $N_{\max} > 14$ and for $N_{\min} \leq N \leq 18$ with $N_{\min} < 14$. We find $C_s = (0.020 \pm 0.006)J^2$ indicating a finite Drude weight in the thermodynamic limit. This result is slightly smaller than the data reported in Ref. 33 ($C_s = (0.046 \pm 0.005)J^2$ there for $N = 6, 8, \dots, 14$) but the latter is regained if we use our data for $N = 6, \dots, 14$. Since we observe $C_s(\Delta, N) = C_s(-\Delta, N)$, this implies $D_s(T > 0) > 0$ for the isotropic, ferromagnetic chain also.

The results from the extrapolation are summarized in Fig. 7 (b) together with our data for $N = 17$ and $N = 18$. The plot suggests that (i) $D_s(T) > 0$ for $\Delta = 1$ and (ii) $D_s(T) = 0$ for $\Delta \geq 1.5$ within our numerical accuracy. Respective conclusions can be drawn for $\Delta \leq -1$ since $C_s(\Delta) = C_s(-\Delta)$. We stress that for intermediate Ising-like anisotropies (i.e., $1 < \Delta < 1.5$) the system sizes may still be too small for an unambiguous confirmation of the conjecture^{29,32,36} $D_s(\Delta > 1) = 0$. In particular, the possibility of a finite Drude weight in the gapped regime cannot be ruled out on the basis of the numerical data even though the Drude weight is zero at $T = 0$. An example for such a scenario (i.e., $D_s(T = 0) = 0$ but

$D_s(T > 0) > 0$) has been given in Ref. 35.

Very recently, Long et al.⁴⁴ have applied a newly developed finite-temperature Lanczos method to compute $C_s(N)$ for $N = 24, 26, 28$. Compared to our data, their results strongly deviate from the fits to Eq. (36) for systems with $N \leq 18$ for all values of Δ presented in Fig. 7 (a).

V. NONINTEGRABLE MODELS

In this section we address the issue of transport in non-integrable models by means of bosonization and exact diagonalization. As discussed in Sec. IIIB, both the spin-current and heat-current operators are not conserved in the presence of frustration and dimerization except for the case of a dimerized XY chain¹⁸.

The original conjecture by Zotos and co-workers²⁷⁻²⁹ stated that the Drude weights are expected to vanish in nonintegrable models and we will argue in the following that our exact diagonalization study corroborates this statement.

In a first numerical work by Alvarez and Gros¹⁵ on thermal transport, the data obtained by complete and exact diagonalization of systems with $N \leq 14$ have been interpreted in favor of a nonzero Drude weight $D_{th}(T > 0) > 0$ in the cases of spin ladders and frustrated spin chains. However, we have argued^{17,21} that this conclusion cannot be sustained for the case of gapped, frustrated chains if larger systems of up to 18 sites and additional values for the next-nearest-neighbor frustration α ($\alpha = 0.35, 0.5, 1$) are included in the finite-size analysis.

Additionally, several authors have recently used analytic approaches to compute the Drude weight D_{th} ^{18,20} and the spin Drude weight D_s ⁴³ in the low-energy limit. If the effective model describes non-interacting particles such as in Ref. 18 in the case of the spin ladder, a finite Drude weight will naturally exist. However, to prove that the Drude weight is also finite in the corresponding lattice model is more difficult. The outcome of a low-energy description crucially depends on the effective models, i.e., one has to take care which operators are kept and which ones can be omitted when passing from the lattice to the continuum limit. In particular, Rosch and Andrei³⁸ have shown that two independent incommensurate umklapp terms suffice to relax the spin current in massless models. Since this result has not been fully appreciated by some of the aforementioned papers, we will discuss the line of reasoning of Ref. 38 and apply these ideas to the models which are of interest in this paper. We will argue that a vanishing Drude weight for both kinds of transport is expected in generic nonintegrable (massive) models also. Thus, the first part of this section will be devoted to the discussion of transport properties in the continuum limit.

In Secs. VB and VC, we will complete our numerical investigation of both the thermal and the spin Drude weight of frustrated and dimerized spin systems with ar-

bitrary values of α and λ . The main focus will be on the finite-size analysis of the high-temperature prefactor $C_{th[s]}(N)$ (see Eq. (20)). If not stated otherwise, $\Delta = 1$.

A. Bosonization

The low-energy description of the systems studied below, i.e., dimerized chain and frustrated chains, can be cast in the general form of a $U(1)$ scalar field theory, known as a Luttinger liquid (denoted by H_{LL}), with a perturbation g corresponding to a relevant operator H_{rel} plus all irrelevant operators H_{irr} allowed by the symmetries of the given problem⁶⁴

$$H = H_{LL} + H_{rel} + H_{irr}, \quad (38)$$

$$H_{LL} = \int dx \left(vK(\partial_x \Theta)^2 + \frac{v}{K}(\partial_x \phi)^2 \right), \quad (39)$$

$$H_{rel} = g \int dx \cos(\alpha\phi). \quad (40)$$

$\phi = \phi(x, \tau)$ is a bosonic field in 1+1 dimensions and Θ is the dual field $\partial_x \Theta = (1/K)\partial_\tau \phi$. K is the Luttinger parameter and v is the velocity. General situations involving more than one relevant operator could also occur, but this does not change the discussion below.

The Hamiltonian, Eq. (38), with $H_{irr} \equiv 0$ corresponds either to a Luttinger liquid in a generic massless situation ($g = 0$, e.g., the massless regime of the frustrated chain) or to a sine-Gordon theory in the massive cases ($g \neq 0$, e.g., dimerized chain, massive regime of the frustrated chain). These descriptions provide in general the correct low-energy picture if one is interested in, e.g., the long-distance behavior of correlators, and usually, one can discard the irrelevant terms H_{irr} since they only contribute with subleading corrections.

However, as was pointed out in Ref. 38, certain operators have a crucial effect on transport properties and should therefore be taken into account to reproduce the correct low-frequency and low-temperature behavior even if these operators are irrelevant in the renormalization group sense. The main result of Ref. 38 is that a certain class of incommensurate umklapp operators lead to the decay of all currents and hence render all conductivities finite. The emerging picture is that, except for very special circumstances which could happen in certain integrable models, one should expect a vanishing Drude weight and hence a finite conductivity.

It should be stressed that Ref. 38 is devoted to massless cases, that is, to those situations where no relevant operators are present ($g = 0$ in Eq. (40)). However, one can argue that the main ingredient in the proof, that is, the violation of all conservation laws due to the presence of incommensurate umklapp operators, is independent of the scaling dimensions of the operators involved. Hence one could expect a similar picture in the massive case, while clearly the results for $\kappa[\sigma](\omega)$ will be quantitatively different. This conjecture is in full agreement with our

numerical findings.

For pedagogical reasons let us briefly summarize the main results of Ref. 38: among the infinitely many irrelevant operators contained in H_{irr} , those which could produce a decay of the currents are the incommensurate umklapp operators, which are, in the case of pure spin models, generically of the form

$$\int dx \mathcal{O}_{n,m}(x) = \int dx g_{nm} \cos(\sqrt{2\pi}n\phi + k_{nm}x). \quad (41)$$

g_{nm} are coupling constants, $k_{nm} = 2nk_F - mG$ where k_F is the Fermi momentum, and G is a reciprocal lattice vector. In a fermionic representation, n is the number of fermions which change chirality under the action of the operator $\mathcal{O}_{n,m}(x)$.

These operators do not modify the low-energy expressions for the energy and spin current. The same holds for the relevant operator²⁰ in Eq. (40). The currents take the form (see, e.g., Refs. 17,65)

$$j_s = \frac{-vK}{\sqrt{2\pi}} \int dx \partial_x \Theta, \quad (42)$$

$$j_{\text{th}} = v^2 \int dx \partial_x \phi \partial_x \Theta. \quad (43)$$

Comparing our notation with Ref. 38, note that $j_s \sim J_0$ and $j_{\text{th}} \sim P_T$. The spin current neither commutes with the relevant operator nor with H_{irr} while for the thermal current, $[H_{\text{rel}}, j_{\text{th}}] = 0$ but $[H_{\text{irr}}, j_{\text{th}}] \neq 0$.

The key observation³⁸ is that in the presence of *one* such operator $\mathcal{O}_{n,m}(x)$, there is still a conserved current which can be written as a linear combination of the spin and thermal current

$$j_{\text{conserved}} = k_{nm}j_s + 2nj_{\text{th}}. \quad (44)$$

However, as soon as *more* than one of the operators $\mathcal{O}_{n,m}(x)$ are considered, no conservation law of the type (44) survives and hence the conductivity is expected to be finite. Since there is no reason *a priori* to exclude such incommensurate operators, this seems to be the generic situation. As incommensurate operators have been considered neither in Ref. 18 nor in Ref. 20 it is not clear whether their results of a finite thermal Drude weight in the low-energy limit provide a proof of $D_{\text{th}}(T > 0) > 0$ for the respective nonintegrable lattice models.

Generally, even if the current operator is not conserved, a nonzero Drude weight can be caused by the existence of (nontrivial) conserved quantities $\{Q_I\}$ with a finite projection on the current operator $j_{\text{th}[s]}$ in the Liouville space (see, e.g., Refs. 38,46,47,57). More precisely, the Drude weight is nonzero if

$$D_{\text{th}[s]}(T) = \frac{\pi}{T2[1]N} (j_{\text{th}[s]} | \mathcal{P} j_{\text{th}[s]}) > 0 \quad (45)$$

where \mathcal{P} is the projection operator on *all* conserved quantities $\{Q_I\}$. $(A | B)$ denotes Mori's scalar product⁵⁷ in the

space of operators

$$(A(t) | B) = \frac{1}{\beta} \int_0^\beta d\tau \langle A(t)^\dagger B(i\tau) \rangle. \quad (46)$$

Under certain circumstances, e.g., integrability, it is possible to construct an infinite set of $\{Q_I\}$ (see Ref. 30 and references therein). Still, the evaluation of Eq. (45) is a nontrivial problem.

In the literature^{30,43}, one often refers to a weaker condition than Eq. (45), namely Mazur's inequality^{30,66} where a subset of the $\{Q_I\}$ or even only one operator $Q_i \in \{Q_I\}$ is taken into account. Therefore, Mazur's inequality provides a lower bound for the Drude weight. For instance, the conservation law³⁸, Eq. (44), would suffice to prove that $D_s > 0$ if no further incommensurate operators are considered.

Quite recently, such an operator Q_i has been found for charge transport in a Luttinger-liquid plus interactions spoiling both the integrability and the conservation of the spin current operator⁴³, reformulating Zotos and co-workers's results from Ref. 30 in the continuum limit. The conserved quantity can be readily identified as the thermal current operator (compare Refs. 17,20). However, their proof of $(j_s | Q_i) > 0$ assumes particle-hole symmetry to be broken, e.g., by the existence of a magnetic field (see also Refs. 22,30). Consequently, for the class of models considered in Ref. 43, a nonzero Drude weight can be inferred. Since the incommensurate operators of Eq. (41) are explicitly excluded in Ref. 43, their result does not contradict our numerical indications for a vanishing Drude weight D_s in nonintegrable spin-lattice models.

B. Thermal transport in nonintegrable models

Frustrated chain - In the thermodynamic limit, the low-energy spectrum of a frustrated chain with $\alpha < \alpha_{\text{crit}} \approx 0.241$ ⁶⁷ is gapless and gapped for $\alpha > \alpha_{\text{crit}}$. The thermal Drude weight in the gapped regime of frustrated chains has been discussed in detail in Refs. 17,21 where we found clear indications of a vanishing Drude weight for $N \rightarrow \infty$. Figure 8 shows the thermal Drude weight $D_{\text{th}}(N, T)$ and the specific heat C_V for $\alpha = 0.2$ and $N = 8, 10, 12, 14, 16, 18$. For chains of finite length, the data at low temperatures are dominated by the finite-size gap. Hence the Drude weight and specific heat are exponentially suppressed for small T . While the specific heat converges to the thermodynamic limit at temperatures $T \gtrsim 0.25J$, strong finite-size effects are present in the data for the Drude weight at all temperatures.

At low temperatures, $D_{\text{th}}(N, T)$ monotonically increases with system size similar to the case of $\alpha = 0.35$ (see Fig. 3 in Ref. 17). In Ref. 21, we have argued that the notion of an increasing Drude weight at low

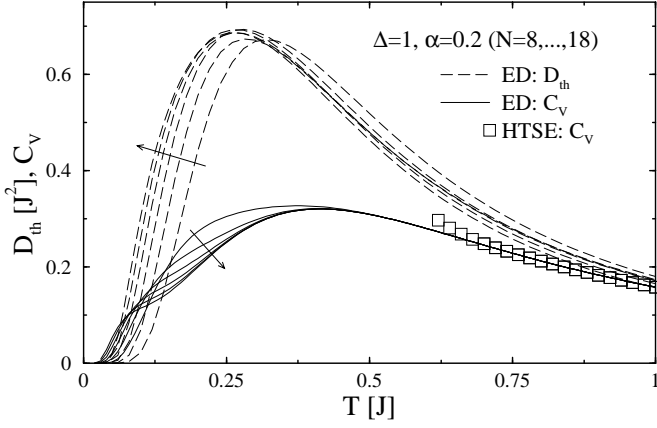


FIG. 8: Thermal transport, frustrated chain: Drude weight $D_{\text{th}}(N, T)$ (dashed lines) and specific heat C_V (solid lines) for $\alpha = 0.2$ and $N = 8, \dots, 18$ sites (arrows indicate increasing system size). The plot includes data for C_V from a high-temperature series expansion (HTSE) reproduced from Ref. 68 (note that only the bare high-temperature series up to order 10 in J/T is shown). By means of extrapolation schemes, the HTSE can be extended to significantly lower temperatures, see Ref. 68).

temperatures does not support the conjecture¹⁵ of a finite D_{th} for $N \rightarrow \infty$ for $\alpha = 0.35$. In fact, we have shown that a crossover temperature T^* which we define by $D_{\text{th}}(N+2, T^*) = D_{\text{th}}(N, T^*)$ and even N seems to extrapolate to zero as a function of system size. This implies that the temperature range where one observes an increasing Drude weight with system size could vanish for $N \rightarrow \infty$. An analogous finite-size analysis of T^* for $\alpha = 0.2$ (not shown in the figures) could also be interpreted in the same sense, i.e., the temperature interval where $D_{\text{th}}(N, T) < D_{\text{th}}(N+2, T)$ tends to vanish for $N \rightarrow \infty$. To summarize the discussion of the low-temperature regime, we emphasize that the finite-size data should not be used to speculate about the thermodynamic limit.

In Fig. 9 (a), we present the high-temperature prefactor $C_{\text{th}}(N)$ for several values of α both in the gapless ($\alpha = 0.1, 0.2$, open symbols) and the gapped regime ($\alpha = 0.25, 0.35, 0.5, 1$, solid symbols; the last three sets have already been shown in Ref. 21). Finite systems with up to $N = 18$ sites have been analyzed. While $C_{\text{th}}(N)$ appears to be almost constant in the case of $\alpha = 0.1$, a substantial decrease with system size is observed for larger α and sufficiently large N as it is especially obvious for $\alpha = 1$. We also note that, regarding thermal transport, the data at the Majumdar-Ghosh point $\alpha = 0.5$ (see Ref. 69 and references therein) do not point to any peculiarities.

In panel (b) of Fig. 9, $C_{\text{th}}(N)$ is plotted versus α for $N = 14, 16, 18$. Starting at small α , we observe that $C_{\text{th}}(N)$ is discontinuous at $\alpha = 0$ which will be commented below. The curve further decreases with α and exhibits a minimum at $\alpha \approx 0.4$ for $N = 14$ and $\alpha \approx 0.5$

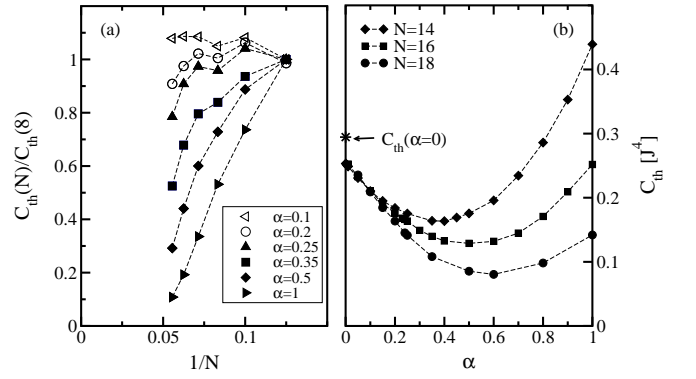


FIG. 9: Thermal transport: high-temperature prefactor $C_{\text{th}}(N)$ for frustrated chains. Panel (a): $C_{\text{th}}(N)/C_{\text{th}}(8)$ versus $1/N$ for various values of α both in the gapless and gapped regime ($N = 8, \dots, 18$) (see also Ref. 21). Panel (b): $C_{\text{th}}(N)$ for $N = 14, 16, 18$ as a function of frustration α . The arrow indicates the system size independent value of C_{th} at $\alpha = 0$.

for $N = 16$. The position of the minimum seems to be further shifted towards larger α on growing N . Further increasing the next-nearest-neighbor interaction drives the system into the limit of two decoupled chains each with $N/2$ sites and interchain interaction α . Exactly for $J \rightarrow 0; J\alpha = \text{const}$, the current operator is again conserved. Consequently, one expects the Drude weight to increase for large α at finite and fixed N . This feature is indeed found for $\alpha \gtrsim 0.5$, see Fig. 9 (b).

Fig. 9 (b) indicates a difference between the gapped and gapless regimes: the decrease of $C_{\text{th}}(N)$ with N is weaker in the gapless regime. We suggest the following two scenarios for further discussion: (i) the Drude weight is nonzero in the gapless regime and zero in the gapped regime; (ii) the Drude weight is zero for all $\alpha > 0$, but, depending on α , there is a characteristic system size $N(\alpha)$ with $C_{\text{th}}(N) \approx \text{const}$ for $N < N(\alpha)$ and monotonically decreasing for $N > N(\alpha)$.

The first interpretation might be plausible in view of the significant differences in the low-energy properties for $\alpha < \alpha_{\text{crit}}$ and $\alpha > \alpha_{\text{crit}}$. However, since C_{th} is essentially the Drude weight at *infinite* temperature where all states contribute with equal weight, it is not clear why low-energy features should play a crucial role for the finite-size scaling in the limit $\beta \rightarrow 0$.

A second objection against the first scenario arises from the analysis of the level-spacing distribution both in the gapped and gapless regime. Exploiting translational invariance and conservation of total S_{tot}^z already lifts all degeneracies on finite systems as is obvious from Fig. 10 showing the integrated level spacing distribution $I(\epsilon)$; see Eq. (32). The difference to the spectrum of the integrable model (see Fig. 3) is striking: while a large fraction of states with $\Delta E_n < 10^{-8}J$ is present for $\Delta = 0.5, \alpha = 0$, no such candidates for degenerate states appear in the case of $\alpha = 0.2, \Delta = 1$. This feature is characteristic for $\alpha > 0$ which, in particular, supports the conjecture that transport properties in the

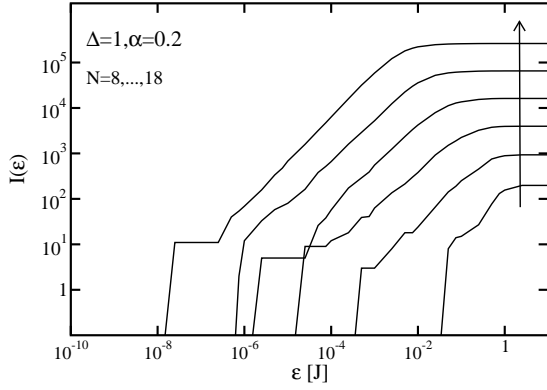


FIG. 10: Frustrated chain: distribution of level spacings in the spectrum of finite chains with $8 \leq N \leq 18$ (bottom to top as indicated by the arrow) for $\alpha = 0.2$. ΔE_n is the difference of adjacent energy levels in subspaces classified by total S_{tot}^z and momentum k . The number $I(\epsilon)$ of ΔE_n with $\Delta E_n < \epsilon$ summed over all subspaces is plotted versus ϵ .

gapped and gapless regimes should not be different at high temperatures. Exceptions are found for $\alpha = 0.5, 1$. At the Majumdar-Ghosh point, one degenerate state occurs if $N/2$ is even. In the latter case (i.e., $\alpha = 1$), there are degenerate states in the spectra of chains with $N = 10, 12, 14, 18$ which are, however, small in number (≈ 10 for $N = 18$).

Next, there is the discontinuity of $C_{\text{th}}(N)$ at $\alpha = 0$. A small, but finite frustration (e.g., $\alpha = 10^{-4}, 10^{-3}$) has the effect that degeneracies are lifted while the values of diagonal matrix elements $|\langle n | j_s | n \rangle|^2$ are almost unaffected. This leads to the substantial difference between C_{th} at $\alpha = 0$ compared to small, but finite $\alpha > 0$. Finally, we mention that the fact of $C_{\text{th}}(N) \approx \text{const}$ for small α could be a consequence of the proximity to the integrable point $\alpha = 0$.

In conclusion, our numerical data indicate a vanishing thermal Drude weight for arbitrary values of α at high temperatures. This result is difficult to reconcile with the recent findings^{18,20} of a nonzero Drude weight in the continuum limit as we have discussed above that a crossover from a nonzero to a zero Drude weight as a function of temperature is not likely.

Spin ladder and dimerized chain - Now we turn to the cases of the dimerized chain and the spin ladder. First, we discuss the numerical data for the thermal Drude weight $D_{\text{th}}(N, T)$ taking the example of a spin ladder with $\alpha = J_{\parallel}/J_{\perp} = 0.5, J_{\perp} = J$ for $N = 8, 10, 12, 14, 16$. Second, the results from a finite-size analysis of the high-temperature prefactor for both spin ladders and dimerized chains are presented. Finally, we comment on possible implications of our results for the interpretation of recent experiments³.

Due to the dimerization, the unit cell of our model is doubled restricting the maximal system size to $N = 16$

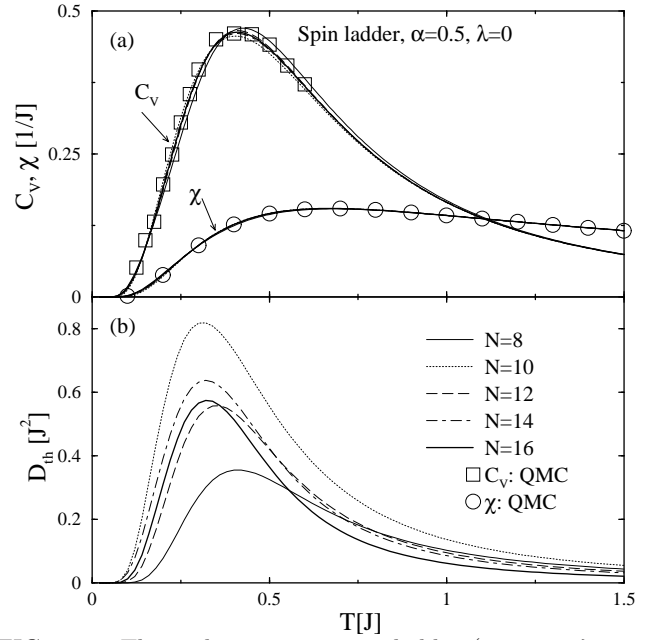


FIG. 11: Thermal transport, spin ladder ($\alpha = 0.5, \lambda = 0, N = 8, \dots, 16$). Panel (a): specific heat C_V and susceptibility χ . Panel (b): Drude weight $D_{\text{th}}(N, T)$. ED for D_{th}, C_V, χ : lines; QMC for $C_V(\chi)$: squares(circles) reproduced from Ref. 15(70).

in our numerical computations at present.

Regarding the level-spacing distribution, degeneracies are still present in the case of the spin ladder. For example, there are $\lesssim 10^2$ degenerate states for $N = 16$ compared to $\gtrsim 10^3$ in the integrable case (see Fig. 3). The spectra of dimerized chains show the same features.

The specific heat C_V , the susceptibility χ , and the thermal Drude weight $D_{\text{th}}(N, T)$ are plotted versus T in Fig. 11 for $N = 8, 10, 12, 14, 16$ and $\alpha = 0.5, \lambda = 0$ (panel (a): C_V, χ , panel (b): $D_{\text{th}}(N, T)$). The main characteristics are the following: (i) for the specific heat, finite-size effects are small and negligible for the susceptibility; (ii) the data for $D_{\text{th}}(N, T)$ display strong finite-size effects at all temperatures; (iii) $D_{\text{th}}(N, T)$ is monotonically decreasing at high temperatures for $N > 8$ and $T \gtrsim 0.6J$; (iv) the positions of the maxima of the specific heat and the Drude weight are different; (v) for $N/2$ even(odd), the data are monotonically increasing(decreasing) at low temperatures. The latter may be attributed to the fact that $D_{\text{th}}(N, T)$ is diverging for decoupled chains and odd N .

It should be stressed that the restricted number of system sizes analyzed here precludes any conclusions from the finite-size scaling at temperatures $T \lesssim 0.6J$; in particular, since the N -dependence is nonmonotonic. Note that even a monotonic increase of $D_{\text{th}}(N, T)$ with system size at low T as observed in the case of frustrated chains with, e.g., $\alpha = 0.35$ does not unambiguously point to a finite Drude weight (see the discussion of $D_{\text{th}}(N, T)$ of frustrated chains and Ref. 21).

While our numerical data for the specific heat are in

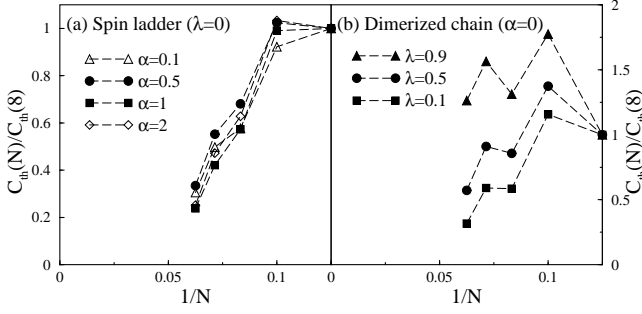


FIG. 12: Thermal transport: $C_{\text{th}}(N)$ for spin ladders (panel (a)) and dimerized chains (panel (b)). Data are shown for $N = 8, \dots, 16$ spins (i.e., ladders with $4, \dots, 8$ rungs).

quantitative agreement with the results from Ref. 15 for the same choice of parameters, only qualitative consistency is found for the thermal Drude weight regarding points (ii)-(iv). Note that the Drude weight D_{th} in Ref. 15 is measured in units of $J_{\parallel} \sim \alpha J$ instead of $J_{\perp} = J$ used in this work. The specific heat, however, is dimensionless. Also, compared to point (v), the opposite monotony behavior is observed at low temperatures in Ref. 15. One may speculate that this difference is due to the use of twisted boundary conditions and different definitions for the energy-current operator j_{th} in Ref. 15.

The finite-size analysis of the high-temperature prefactor $C_{\text{th}}(N)$ reveals a systematic decrease with system size for $N > 8$ both for the case of the spin ladder and dimerized chain as it is evident from Fig. 12. In particular, by normalizing the data on the respective values for $C_{\text{th}}(N = 8)$ the finite-size dependence of the data for the spin ladder (panel (a) in Fig. 12) appears to be almost independent of the interchain coupling $\alpha = J_{\parallel}/J_{\perp}$ for the choice of parameters considered here ($\alpha = 0.1, 0.5, 1, 2$) including the isotropic ladder ($\alpha = 1$). Only the results for the dimerized chain with $\lambda = 0.9$ show less evidence for a vanishing of C_{th} . This does, however, not question the conclusion of a vanishing thermal Drude weight because $\lambda = 0.9$ is still very close to the homogeneous Heisenberg chain where $D_{\text{th}}(T > 0)$ is finite.

To summarize the finite-size analysis, one can conclude that the numerical data for D_{th} of spin ladders and dimerized chains indicate a vanishing Drude weight for $N \rightarrow \infty$. In particular, this includes the isotropic spin ladder ($J_{\perp} = J_{\parallel}; \alpha = 1$) which is of relevance because the magnetic properties of $\text{La}_5\text{Ca}_9\text{Cu}_{24}\text{O}_{41}$ are well described by $J_{\perp} \approx J_{\parallel}$ ^{71,72}.

Recently, first attempts have been made to extract magnetic mean free paths l_{mag} from the experimental data for the magnetic part κ_{mag} of the thermal conductivity of $\text{La}_5\text{Ca}_9\text{Cu}_{24}\text{O}_{41}$. Assuming that heat is carried mainly by the elementary excitations of spin ladders (i.e., dispersive triplet modes) Hess et al.⁵ have used a relaxation time ansatz for the respective kinetic equation

reading

$$\kappa_{\text{mag}} = \sum_k C_{V,k} v_k l_k. \quad (47)$$

Here, $C_{V,k}$ is the specific heat per k -space volume, v_k is the triplet dispersion, and l_k the momentum-dependent mean-free path. This approach results in very large mean-free paths l_{mag} of the order of 3000\AA at 100K corresponding to ≈ 770 lattice constants. Following this work, Alvarez and Gros¹⁵ have suggested a much smaller value for l_{mag} , namely, $176\text{\AA} \approx 45$ lattice constants at $T = 100\text{K}$. They have attributed this significant difference to the fact that $D_{\text{th}}(N, T) \not\sim C_V$ as is seen in the numerical data. It is, however, straightforward to check that Eq. (47) leads to $\kappa_{\text{mag}} \not\sim C_V$, implying that this alone does not explain the different values found for l_{mag} in Refs. 3,15.

The result for l_{mag} of Ref. 15 is explicitly based on the assumption of a *finite* Drude weight D_{th} for spin ladders which is questionable in view of the detailed numerical results presented in this paper.

C. Spin transport in nonintegrable models

In this last section, we give an overview of our results for the Drude weight for spin transport in nonintegrable models. The dependence of D_s on frustration and dimerization will be systematically discussed. Our analysis of the Drude weight at finite temperatures includes next-nearest-neighbor interactions $\sum_i \vec{S}_i \cdot \vec{S}_{i+2}$ extending previous numerical studies of nonintegrable lattice models^{29,33,41} where different kinds of Ising-like interactions ($\sum_i S_i^z S_{i+2}^z$; $i = 2, 3$) have been considered. Note in this context that frustration cannot be treated with QMC simulations due to the sign problem⁴¹.

Frustrated chain - Results for the Drude weight $D_s^{I,II}(N, T)$ are shown in Fig. 13 for $\alpha = 0.2$ (main panel) and $\alpha = 0.5$ (inset). In the gapless regime ($\alpha < \alpha_{\text{crit}}$), the finite-size data display features similar to the XXZ model: (i) $D_s^{I,II}(N, T = 0) > 0$; (ii) $D_s^{I,II}(N, T) \approx \text{const}$ at small temperatures; (iii) $D_s^I(N, T) \simeq D_s^{II}(N, T)$ at high temperatures, but significant deviations at low temperatures; (iv) a monotonic decrease with system size at high temperatures $T \gtrsim 0.5J$. Similar to the case of the thermal Drude weight of frustrated chains, we observe that for even N , the monotonic decrease of $D_s^{I,II}(N, T)$ with system size at high temperatures changes to an increase at lower T . However, the temperature, where this change in the monotony behavior occurs, is strongly shifted to lower temperatures as N grows; see Fig. 13. This resembles the case of $D_{\text{th}}(N, T)$ for $\alpha = 0.35$ discussed in Ref. 21 and we conclude that the numerical data for D_s at low temperatures do not give unambiguous evidence for a finite Drude weight.

The observation of $D_s^{I,II}(N, T = 0) > 0$ for small α has also been reported in Ref. 26. There, using the Lanczos

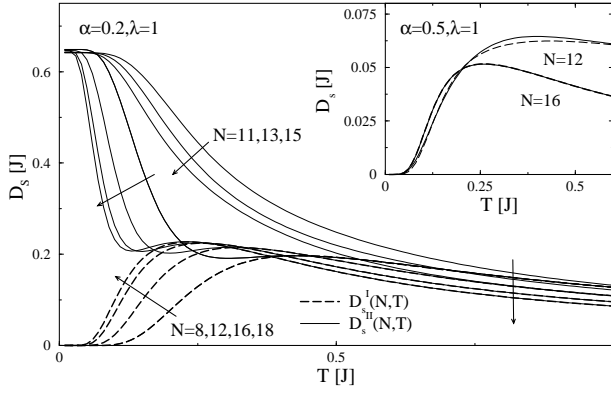


FIG. 13: Spin transport, frustrated chain: Drude weight $D_s^{I,II}(N, T)$ for $N = 8, 11, 12, 13, 15, 16, 18$ and $\alpha = 0.2, \lambda = 1$ (dashed lines: $D_s^I(N, T)$; solid lines: $D_s^{II}(N, T)$). Arrows indicate increasing systems size. Inset: Drude weight at the Majumdar-Ghosh point ($\alpha = 0.5, \lambda = 1$) for $N = 12, 16$.

method and truncation in the $S_{\text{tot}}^z = 0$ subspace, a nonzero Drude weight at $T = 0$ has been found for $\alpha < 0.43$ and $N = 20$. To clarify whether $D_s(T = 0) > 0$ survives in the thermodynamic limit, one should exploit Kohn's formula for $T = 0$ using, e.g., the Lanczos algorithm, which is, however, not the purpose of the present paper.

Consistent with Ref. 26, we find $D_s^{II}(N, T = 0) = 0$ in the case of $\alpha = 0.5$ (see inset of Fig. 13). Notice that $D_s^I(N, T) \simeq D_s^{II}(N, T)$ at all temperatures for $N = 16$. We now turn to the question of a nonzero Drude weight in the thermodynamic limit by a finite-size analysis of the high-temperature prefactor $C_s(N)$. $C_s(N)$ is plotted versus $1/N$ in Fig. 14 (a) for $\alpha = 0.2, 0.35, 0.5, 1$. First, $C_s(N)$ monotonically decreases with system size (except for odd-even effects) for all values of α presented here and exhibits a discontinuity at $\alpha = 0$ analogous to $C_{\text{th}}(N)$ (see inset of Fig. 14). Second, the data for $\alpha = 0.2$ may in principle be extrapolated to a finite value in the thermodynamic limit (see, however, remarks below). The behavior for $\alpha > \alpha_{\text{crit}}$ is similar to the case of the thermal Drude weight since $C_s(N)$ decreases rapidly with N and faster than $1/N$.

Another remarkable difference between the gapped and the gapless regime is revealed in Fig. 14 (b) where we show $C_s(N)$ as a function of frustration α for $N = 14, 16, 18$. In contrast to the thermal Drude weight (see Fig. 9), $C_s(N)$ first grows with α and exhibits a maximum around $\alpha \approx 0.2$. For larger $\alpha \gtrsim 0.7$, $C_s(N)$ increases with α again analogous to the case of the thermal Drude weight (see Fig. 9).

We interpret the data for $\alpha > \alpha_{\text{crit}}$ in terms of a vanishing Drude weight for $N \rightarrow \infty$. For the gapless regime, the possibility for a nonzero C_s cannot be ruled out by our data although the absence of degeneracies (see Fig. 10) supports the conclusion of $C_s = 0$ for all $\alpha > 0$.

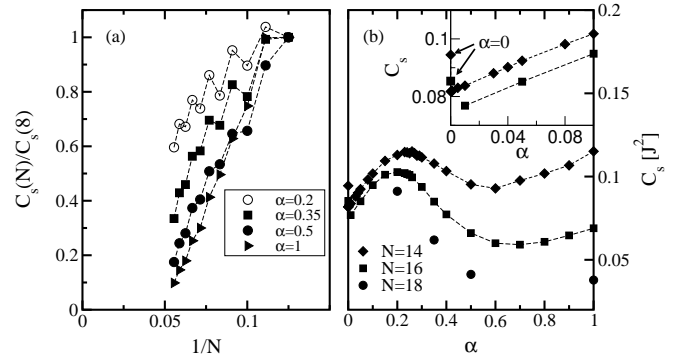


FIG. 14: Spin transport: high-temperature prefactor $C_s(N)$ for frustrated chains. Panel (a): $C_s(N)/C_s(8)$ versus $1/N$ for various values of α both in the gapless and gapped regime ($N = 8, 9, \dots, 18$). Panel (b): $C_s(N)$ for $N = 14, 16, 18$ as a function of frustration α . The inset shows a blowup for small α and $N = 14, 16$.

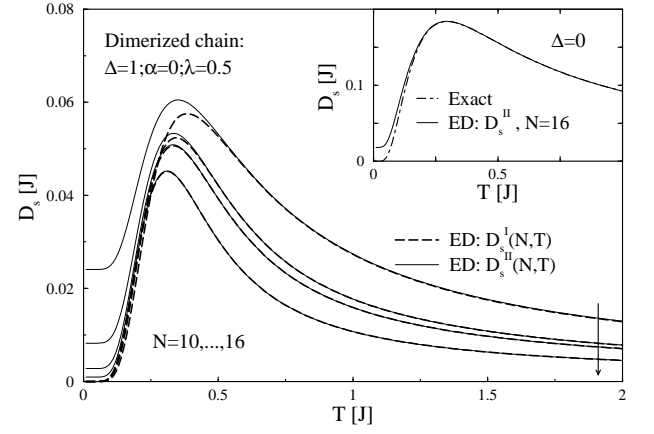


FIG. 15: Spin transport, dimerized chain: Drude weight $D_s^{I,II}(N, T)$ for $N = 10, \dots, 16$ (top to bottom as indicated by the arrow) and $\alpha = 0, \lambda = 0.5$ (dashed lines: $D_s^I(N, T)$; solid lines: $D_s^{II}(N, T)$). In the inset, the exact result from Eq. (50) (dot-dashed line) for the Drude weight of a dimerized XY chain with $\Delta = 0, \alpha = 0, \lambda = 0.5$ and numerical data (solid line) for $N = 16$ sites are shown.

Dimerized chain, spin ladder - While for the frustrated chain and the spin ladder the fermionized Hamiltonian, Eq. (5), contains interaction terms even at $\Delta = 0$, the case of the dimerized XY model, ($\Delta = 0, \lambda \neq 1, \alpha = 0$) corresponds to a model of free, but massive fermions which can be solved exactly (see, e.g., Ref. 18). We will start with a discussion of this limiting case where a finite Drude weight D_s exists.

The Hamiltonian in terms of spinless fermions (see Eq. (5)) reads

$$H^{XY} = \sum_l \frac{\lambda_l}{2} (c_{l+1}^\dagger c_l + \text{H.c.}) \quad (48)$$

($\lambda_l = \lambda$ for l even and $\lambda_l = 1$ otherwise). A straightfor-

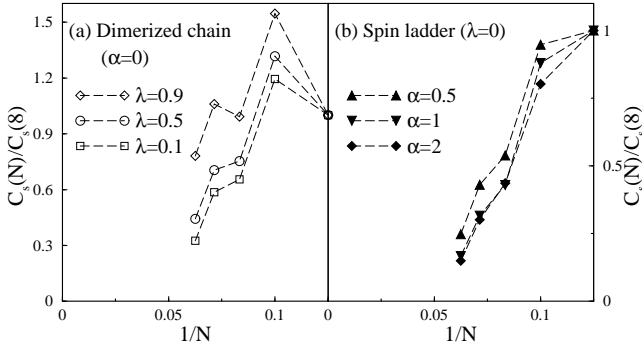


FIG. 16: Spin transport: high-temperature prefactor $C_s(N)$ of the Drude weight for the dimerized chain (panel (a)) and the spin ladder (panel (b)); both for $N \leq 16$.

ward computation diagonalizes H^{XY} (see, e.g., Ref. 18 for details)

$$H^{XY} = \sum_k \epsilon_k (a_{k,+}^\dagger a_{k,+} - a_{k,-}^\dagger a_{k,-}), \quad (49)$$

leading to two modes with a gapped dispersion $\epsilon_k = J\sqrt{(1-\lambda)^2/4 + \lambda \cos(k)}$. Obviously, the spin-current operator $j_s = \sum_k v_k (a_{k,+}^\dagger a_{k,+} - a_{k,-}^\dagger a_{k,-})$ is conserved and the Drude weight can be computed exactly

$$D_s(T) = \frac{1}{4T} \int dk \frac{v_k^2}{\cosh^2[\epsilon_k/(2T)]}. \quad (50)$$

$v_k = \partial \epsilon_k / \partial k$ is the velocity.

In Fig. 15, the Drude weight on finite systems is plotted for a dimerized chain with $\lambda = 0.5$ and both $\Delta = 0$ (inset) and $\Delta = 1$ (main panel). In the former case, we see that the numerical data for 16 sites agree with the exact expression for $N \rightarrow \infty$, Eq. (50), at temperatures $T \gtrsim 0.2J$. The same holds for smaller system sizes (not shown in the figure) for high T . This is in contrast to the curves for $\Delta = 1$ (main panel), where no convergence is observed at all temperatures. For $\Delta = 1$, both $D_s^I(N, T)$ (dashed lines) and $D_s^{II}(N, T)$ (solid lines) have been evaluated proving their equivalence at high temperatures. Small systems ($N = 10, 12$) still exhibit a large nonzero value of $D_s^{II}(N, T = 0)$ which rapidly decreases with system size.

The data for the high-temperature prefactor $C_s(N)$ are collected in Figs. 16 (a) (dimerized chain) and (b) (spin ladder). A substantial decrease of $C_s(N)$ with system size is observed for all choices of parameters and $N > 8$, indicating a vanishing Drude weight at high temperatures.

In summary, our numerical data yield evidence for nonballistic spin transport in nonintegrable spin models with a spin gap, i.e., $D_s(T > 0) = 0$ in the thermodynamic limit. This result confirms Zotos and coworker's

original conjecture²⁹ that transport in nonintegrable models should be normal. The system sizes investigated here may, however, be too small to clarify whether the Drude weight is zero or not in the gapless phase of the frustrated chain.

VI. CONCLUSION

In this paper, we have presented a detailed study of the Drude weights for thermal and spin transport in one-dimensional spin systems at finite temperatures. Let us focus here on the main results while more detailed summaries can be found in the preceding sections.

Thermal transport in the XXZ model is generically dissipationless due to the conservation of the energy current operator³⁰. Our data for the thermal Drude weight are in excellent agreement with the Bethe ansatz^{14,49}. For spin transport in this model, we have presented numerical results for various values of the anisotropy. Our data confirm the observation^{29,32,33,37,41,43,44} of a finite Drude weight D_s in the gapless regime ($|\Delta| < 1$). We have discussed some so far unresolved issues: first, the exact temperature dependence of the Drude weight in the critical regime ($|\Delta| < 1$) and, second, the question of whether $D_s(T > 0)$ is finite for the isotropic chain ($\Delta = 1$). Regarding the first point, analytical⁴³ and numerical results⁴¹ are compatible with the finite-size data presented here. Regarding the second issue, the exact diagonalization data of finite systems with $N \leq 18$ do favor a *finite* Drude weight at $\Delta = 1$.

In the case of nonintegrable models (frustrated chain, dimerized chain, spin ladder), our main result is that the finite-size analysis of the ED data does not indicate a finite Drude weight in the thermodynamic limit either for thermal or spin transport, but rather supports the conclusion that transport in these systems is dissipative. While we have concentrated our numerical analysis on the finite-size scaling at high temperatures, this result is corroborated by bosonization in the low-temperature limit.

Acknowledgments - This work was supported by the DFG, Schwerpunktprogramm 1073, and by a DAAD-ANTORCHAS exchange program. It is a pleasure to thank J. V. Alvarez, N. Andrei, B. Büchner, C. Gros, C. Hess, A. Klümper, T. Lorenz, T. M. Rice, and A. Rosch for fruitful discussions. We are indebted to A. Klümper and K. Sakai for sending us their data. We acknowledge support by the Rechenzentrum of the TU Braunschweig where parts of the numerical computations have been performed on a COMPAQ ES45.

- * Electronic address: f.heidrich-meisner@tu-bs.de
- † On leave from Universidad de La Plata and Universidad de Lomas de Zamora, Argentina.
- ¹ Yoichi Ando, J. Takeya, D.L. Sisson, S.G. Doettinger, I. Tanaka, R.S. Feigelson, and A. Kapitulnik, Phys. Rev. B **58**, R2913 (1998); J. Takeya, I. Tsukada, Yoichi Ando, T. Masuda, and K. Uchinokura, *ibid.* **61**, 14700 (2000).
 - ² A. V. Sologubenko, K. Giannò, H. R. Ott, U. Ammerahl, and A. Revcolevschi, Phys. Rev. Lett. **84**, 2714 (2000).
 - ³ C. Hess, C. Baumann, U. Ammerahl, B. Büchner, F. Heidrich-Meisner, W. Brenig, and A. Revcolevschi, Phys. Rev. B **64**, 184305 (2001).
 - ⁴ K. Kudo, S. Ishikawa, T. Noji, T. Adachi, Y. Koike, K. Maki, S. Tsuji, and Ken-ichi Kumagai, J. Phys. Soc. Jpn. **70**, 437 (2001).
 - ⁵ C. Hess, U. Ammerahl, C. Baumann, B. Büchner, and A. Revcolevschi, Physica B **312-313**, 612 (2002).
 - ⁶ A. V. Sologubenko, E. Felder, K. Giannò, H. R. Ott, A. Vietkine, and A. Revcolevschi, Phys. Rev. B **62**, R6108 (2000); A. V. Sologubenko, K. Giannò, H. R. Ott, A. Vietkine, and A. Revcolevschi, *ibid.* **64**, 054412 (2001).
 - ⁷ A. V. Sologubenko, H. R. Ott, G. Dhalenne, and A. Revcolevschi, Europhys. Lett. **62**, 540 (2003).
 - ⁸ Y. Nakamura, S. Uchida, T. Kimura, N. Motohira, K. Kishio, K. Kitazawa, T. Arima, and Y. Tokura, Physica C **185-189**, 1409 (1991).
 - ⁹ M. Hofmann, T. Lorenz, K. Berggold, M. Grüninger, A. Freimuth, G.S. Uhrig, and E. Brück, Phys. Rev. B **67**, 184502 (2003).
 - ¹⁰ C. Hess, B. Büchner, U. Ammerahl, L. Colonescu, F. Heidrich-Meisner, W. Brenig, and A. Revcolevschi, Phys. Rev. Lett. **90**, 197002 (2003).
 - ¹¹ X. F. Sun, J. Takeya, Seiki Komiya, and Yoichi Ando, Phys. Rev. B **67**, 104503 (2003).
 - ¹² C. L. Kane and M. P. A. Fisher, Phys. Rev. Lett. **76**, 3192 (1996).
 - ¹³ K. Saito, S. Takesue, and S. Miyashita, Phys. Rev. E **54**, 2404 (1996).
 - ¹⁴ A. Klümper and K. Sakai, J. Phys. A **35**, 2173 (2002).
 - ¹⁵ J. V. Alvarez and C. Gros, Phys. Rev. Lett. **89**, 156603 (2002).
 - ¹⁶ K. Saito and S. Miyashita, J. Phys. Soc. Jpn. **71**, 2485 (2002).
 - ¹⁷ F. Heidrich-Meisner, A. Honecker, D.C. Cabra, and W. Brenig, Phys. Rev. B **66**, 140406(R) (2002).
 - ¹⁸ E. Orignac, R. Chitra, and R. Citro, Phys. Rev. B **67**, 134426 (2003).
 - ¹⁹ K. Saito, Europhys. Lett. **61**, 34 (2003).
 - ²⁰ K. Saito, Phys. Rev. B **67**, 064410 (2003).
 - ²¹ F. Heidrich-Meisner, A. Honecker, D.C. Cabra, and W. Brenig, cond-mat/0302358 (unpublished).
 - ²² K. Louis and C. Gros, Phys. Rev. B **67**, 224410 (2003).
 - ²³ B.S. Shastry and B. Sutherland, Phys. Rev. Lett. **65**, 243 (1990).
 - ²⁴ R. M. Fye, M. J. Martins, D. J. Scalapino, J. Wagner, and W. Hanke, Phys. Rev. B **44**, 6909 (1991).
 - ²⁵ D. J. Scalapino, S. R. White, and S. C. Zhang, Phys. Rev. Lett. **68**, 2830 (1992); Phys. Rev. B **47**, 7995 (1993).
 - ²⁶ J. Bonča, J. P. Rodriguez, J. Ferrer, and K. S. Bedell, Phys. Rev. B **50**, 3415 (1994).
 - ²⁷ H. Castella, X. Zotos, and P. Prelovšek, Phys. Rev. Lett. **74**, 972 (1995).
 - ²⁸ H. Castella and X. Zotos, Phys. Rev. B **54**, 4375 (1996).
 - ²⁹ X. Zotos and P. Prelovšek, Phys. Rev. B **53**, 983 (1996).
 - ³⁰ X. Zotos, F. Naef, and P. Prelovšek, Phys. Rev. B **55**, 11029 (1997).
 - ³¹ K. Fabricius and B. M. McCoy, Phys. Rev. B **57**, 8340 (1998).
 - ³² F. Naef and X. Zotos, J. Phys.: Condens. Matter **10**, L183 (1998).
 - ³³ B. N. Narozhny, A. J. Millis, and N. Andrei, Phys. Rev. B **58**, R2921 (1998).
 - ³⁴ S. Fujimoto and N. Kawakami, J. Phys. A **31**, 465 (1998).
 - ³⁵ S. Kirchner, H. G. Evertz, and W. Hanke, Phys. Rev. B **59**, 1825 (1999).
 - ³⁶ N. M. R. Peres, P. D. Sacramento, D. K. Campbell, and J. M. P. Carmelo, Phys. Rev. B **59**, 7382 (1999).
 - ³⁷ X. Zotos, Phys. Rev. Lett. **82**, 1764 (1999).
 - ³⁸ A. Rosch and N. Andrei, Phys. Rev. Lett. **85**, 1092 (2000).
 - ³⁹ N. Lafflorencie, S. Capponi, and E. S. Sørensen, Eur. Phys. J B **24**, 77 (2001).
 - ⁴⁰ X. Zotos, J. Low Temp. Phys. **126**, 1185 (2002).
 - ⁴¹ J. V. Alvarez and C. Gros, Phys. Rev. Lett. **88**, 077203 (2002); Phys. Rev. B **66**, 094403 (2002).
 - ⁴² A. Rosch and N. Andrei, J. Low Temp. Phys. **126**, 1195 (2002).
 - ⁴³ S. Fujimoto and N. Kawakami, Phys. Rev. Lett. **90**, 197202 (2003).
 - ⁴⁴ M.W. Long, P. Prelovšek, S. El Shawish, J. Karadamoglou, and X. Zotos, cond-mat/0302211 (unpublished).
 - ⁴⁵ F. Meier and D. Loss, Phys. Rev. Lett. **90**, 167204 (2003).
 - ⁴⁶ W. Brenig, Z. Phys. B **89**, 187 (1992).
 - ⁴⁷ M. Garst and A. Rosch, Europhys. Lett. **55**, 66 (2001).
 - ⁴⁸ Th. Niemeijer and H. A. W. van Vianen, Phys. Lett. **34A**, 401 (1971).
 - ⁴⁹ K. Sakai and A. Klümper, cond-mat/0307227 (unpublished).
 - ⁵⁰ A. Klümper, private communication, and J. Benz, T. Fukui, A. Klümper, and C. Scheeren (unpublished).
 - ⁵¹ S. Glocke, diploma thesis, Universität Dortmund, 2002 (unpublished).
 - ⁵² M. Hofmann, T. Lorenz, A. Freimuth, G.S. Uhrig, H. Kageyama, Y. Ueda, G. Dhalenne, and A. Revcolevschi, Physica B **312-313**, 597 (2002); A. N. Vasil'ev, V. V. Pryadun, D. I. Khomskii, G. Dhalenne, A. Revcolevschi, M. Isobe, and Y. Ueda, Phys. Rev. Lett. **81**, 1949 (1998).
 - ⁵³ G. D. Mahan, *Many-Particle Physics*, Plenum Press, New York, 1990.
 - ⁵⁴ W. Brenig, Phys. Rev. B **56**, 2551 (1997).
 - ⁵⁵ R. Kubo, J. Phys. Soc. Jpn. **12**, 570 (1957).
 - ⁵⁶ J. M. Luttinger, Phys. Rev. **135**, A1505 (1964).
 - ⁵⁷ D. Forster, *Hydrodynamic Fluctuations, Broken Symmetry, and Correlation Functions* (Benjamin, Reading, Mass., 1975).
 - ⁵⁸ W. Kohn, Phys. Rev. **133**, A171 (1964).
 - ⁵⁹ K. Kawasaki, Prog. Theor. Phys. **29**, 801 (1963).
 - ⁶⁰ S. Eggert, I. Affleck, and M. Takahashi, Phys. Rev. Lett. **73**, 332 (1994).
 - ⁶¹ A. Klümper and D. C. Johnston, Phys. Rev. Lett. **84**, 4701 (2000).
 - ⁶² A. Klümper (private communication).
 - ⁶³ Shi-Jain Gu, V. M. Pereira, and N. M. R. Peres, Phys.

- Rev. B **66**, 235108 (2002).
- ⁶⁴ H. J. Schulz, in *Correlated Fermions and Transport in Mesoscopic Systems*, edited by T. Martin, G. Montambaux, and J. Tran Thanh Van (Editions Frontières, Gif-sur-Yvette, 1996), p. 81.
 - ⁶⁵ S. Rao and D. Sen, in *Field Theories in Condensed Matter Physics*, edited by S. Rao (IOP Publishing, Bristol, 2002), cond-mat/0005492.
 - ⁶⁶ P. Mazur, *Physica* (Amsterdam) **43**, 533 (1969); M. Suzuki, *ibid.* **51**, 277 (1971).
 - ⁶⁷ See, e.g., K. Nomura and K. Okamoto, *J. Phys. Soc. Jpn.* **62**, 1123 (1993).
 - ⁶⁸ A. Bühler, N. Elstner, and G.S. Uhrig, *Eur. Phys. J. B* **16**, 475 (2000).
 - ⁶⁹ B.S. Shastry and B. Sutherland, *Phys. Rev. Lett.* **47**, 964 (1981).
 - ⁷⁰ D.C. Johnston, M. Troyer, S. Miyahara, D. Lidsky, K. Ueda, M. Azuma, Z. Hiroi, M. Takano, M. Isobe, Y. Ueda, M.A. Korotin, V.I. Anisimov, A.V. Mahajan, and L.L. Miller, cond-mat/0001147 (unpublished).
 - ⁷¹ M. Matsuda, K. Katsumata, R. S. Eccleston, S. Brehmer, and H.-J. Mikeska, *Phys. Rev B* **62** 8903 (2000).
 - ⁷² M. Windt, M. Grüninger, T. Nunner, C. Knetter, K. P. Schmidt, G. S. Uhrig, T. Kopp, A. Freimuth, U. Ammerahl, B. Büchner, and A. Revcolevschi, *Phys. Rev. Lett.* **87**, 127002 (2001).

In this Erratum, we correct five mistakes in our article Phys. Rev. B **68**, 134436 (2003).

First, there is a typographical error in Eq. (10) ($E_n - E_m$ in the denominator of the second term). The equation should correctly read:

$$D_s^{II}(N, T) = \frac{\pi}{N} \left[\langle -\hat{T} \rangle - \frac{2}{Z} \sum_{\substack{m, n \\ E_m \neq E_n}} e^{-\beta E_n} \frac{|\langle m | j_s | n \rangle|^2}{E_m - E_n} \right].$$

The correct expression was used in the numerical analysis.

Second, on page 5, we state that *Dimerization and frustration which spoil the integrability of the XXZ model also lead to $[H, j_{\text{th}[s]}] \neq 0$ (except for $\Delta = \alpha = 0$)*. This incorrectly implies that $[H, j_s] = 0$ for the dimerized spin-1/2 XY chain. The spin current of the dimerized spin-1/2 XY chain is not conserved since it incorporates inter-band transitions. Yet, the presence of a trivial Drude weight for the free dimerized chain ($\Delta = \alpha = 0$) remains valid simply by virtue of Eqs. (45) and (50) because the intraband current is conserved. See also the inset of Fig. 15 of the original paper, where numerical data are compared to Eq. (50), showing agreement. Our quantitative results for the spin Drude weight of this model are not affected.

Third, on page 15 below Eq. (49), we give an expression for a spin-current operator of the dimerized spin-1/2 XY chain that is conserved. In the sentence "Obviously, the spin current $j_s = \sum_k v_k (a_{k,+}^\dagger a_{k,+} - a_{k,-}^\dagger a_{k,-})$ is conserved ...", the symbol j_s needs to be replaced by j_s^{diag} , denoting the conserved spin current that accounts only for intraband transitions, to distinguish it from the spin-current operator derived in Eq. (24).

Fourth, the numerical data for the spin Drude weight D_s^I for $\Delta = 0.5$ and $N = 8$ presented in Fig. 5(a) of the original paper has a small error due to neglecting accidental degeneracies on this system size. Figure 17 of this Erratum shows Fig. 5 of the original publication including the correct data for D_s^I computed for $N = 8$ in panel (a). This error does not affect the extrapolation of the infinite-temperature Drude weight shown in the inset

of Fig. 5 of the original paper.

Fifth, there is a typographical error in the dispersion relation of a dimerized spin-1/2 XX chain quoted on page 15 below Eq. (49) (missing power of two for the cosine). The correct expression is:

$$\epsilon_k = J \sqrt{(1 - \lambda)^2/4 + \lambda \cos^2(k)}.$$

The correct expression was used in the calculation of the spin Drude weight from Eq. (50) of the original paper.

All these corrections do not affect the discussion and conclusions in the original paper.

We thank J. Hauschild and C. Karrasch for bringing these errors to our attention.

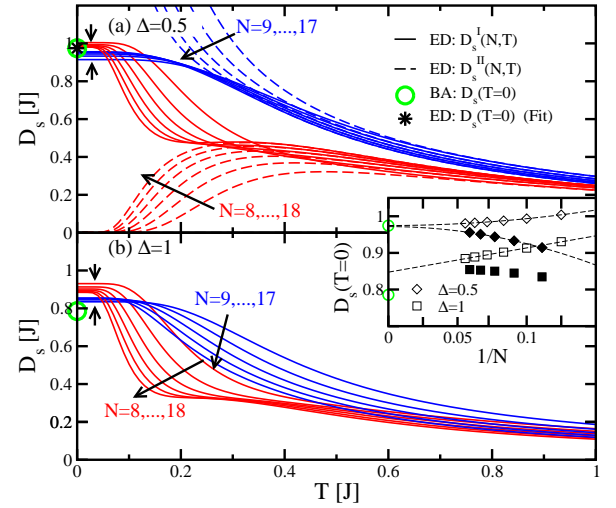


FIG. 17: (Color online) This figure replaces Fig. 5 of the original publication and includes the corrected data for D_s^I computed for $N = 8$.